International Journal of Engineering Science 134 (2019) 1–30

Contents lists available at ScienceDirect

International Journal of Engineering Science

journal homepage: www.elsevier.com/locate/ijengsci

A thermodynamic framework for the modeling of crystallizable triple shape memory polymers

S. Moon, F. Cui, I.J. Rao*

Department of Mechanical & Industrial Engineering, New Jersey Institute of Technology, Newark, NJ 07102, United States

ARTICLE INFO

Article history:
Received 8 September 2017
Revised 21 September 2018
Accepted 8 October 2018
Available online 23 October 2018

Keywords:
Shape memory polymer
Triple shape memory polymer
Multiple natural configuration
Soft active materials
Thermodynamic framework

ABSTRACT

Triple shape memory polymers (TSMPs) can be programed to remember and switch between three distinct shapes with the use of external stimuli, typically an increase in temperature. In this work, constitutive equations have been developed to model the thermo-mechanical behavior of crystallizable TSMPs. In these materials the transient shapes are fixed by the formation of crystalline phases, whereas the switching between the temporary and permanent shapes is due to the melting of the crystalline phases. The model is developed using a framework based on the theory of multiple natural configurations. Constitutive equations have been formulated for the original amorphous phase, the intermediate semi-crystalline phases, and transition of the crystalline phases, during the shape fixation and recovery cycles of TSMPs. These models have been developed within a full thermodynamic framework, extending our previous work in which the models were developed within a mechanical setting (Moon, Cui, & Rao, 2015; Moon, Rao, & Chester, 2016). The model has been applied to solve for the problems of inflation and extension of a hollow cylinder and uniaxial extension. The results are consistent with experimental observations.
© 2018 Elsevier Ltd. All rights reserved.

1. Introduction

Shape memory polymers (SMPs), are stimuli-responsive polymers with the ability to undergo a large recoverable deformation upon stimulation with an external trigger. Dual-shape SMPs change from one shape to another in response to a stimulus. For instance, a complex shape can be deformed in a compacted form by a sequence of heating, deformation, cooling and unloading. Subsequently, a return to the original complex shape can be activated by the application of triggers such as heat, light or exposure to magnetic field to name a few. Triple-shape memory polymers (TSMPs) are a relatively new category of SMPs, in TSMPs three shapes are involved in a shape memory cycle, they can change from a first shape to a second shape and from there to a third shape (Behl & Lendlein, 2012; Behl et al., 2009a; Behl et al., 2009b; Bellin et al., 2006; Hu et al., 2012; Lendlein, Schmidt, & Langer, 2001). This ability of the TSMPs to remember multiple temporary shapes has opened up increasingly complex applications and has served to further motivate the development of shape-memory functions of shape memory polymers (SMPs) (Hu et al., 2012; Hu et al., 2012; Monkman, 2000; Serrano & Ameer, 2012; Xiao, Guo, & Nguyen, 2015; Xie, 2011). For a more detailed discussion of the various potential application of shape memory polymers we refer the reader to the articles (Monkman, 2000; Poilane et al., 2000; Tey, Huang, & Sokolowski, 2001; Tobushi et al., 1996). The thermo-mechanical properties of SMPs can also be easily tailored according to the required application (Baer et al., 2007; Irie, 1998; Kim et al., 1998; Kim, Lee, & Xu, 1996; Mather, Luo, & Rousseau, 2009; Wang & Zhang, 1999).

* Corresponding author.
E-mail address: raoi@njit.edu (I.J. Rao).

https://doi.org/10.1016/j.ijengsci.2018.10.003
0020-7225/© 2018 Elsevier Ltd. All rights reserved.

Heat is used as a trigger in transition from one shape to another in thermo-responsive SMPs (Heuchel et al., 2013; Li et al., 1997; Mather et al., 2009; Srivastava, Chester, & Anand, 2010; Tobushi et al., 1996). Properties of SMPs can be adjusted over a wide range which might enable their application in various fields. As a novel kind of smart material SMPs at present are undergoing rapid growth, researchers have proposed a broad range of potential application areas ranging from biomedicine to outer space. The applications include smart clothing (Hu et al., 2012), medical applications (Baer et al., 2007; Heuchel et al., 2013; Lendlein & Sauter, 2013; Lendlein et al., 2010; Serrano & Ameer, 2012; Srivastava et al., 2010), actuators (Xie, 2011; Heuchel et al., 2013; Zhao, Behl, & Lendlein, 2013) , deployable components and structures in aerospace, smart structural repair, intelligent packing, biosensors, self-repairing auto bodies, hinges, trusses, optical reflectors, morphing skins (Hu et al., 2012; Kim et al., 1998; Kim et al., 1996; Lendlein & Kelch, 2002; Lendlein & Sauter, 2013; Lendlein et al., 2010; Mather et al., 2009; Reyntjens, Du Prez, & Goethals, 1999; Sisson & Lendlein, 2012; Sun et al., 2012; Xie, 2011). SMP cardiovascular stents can facilitate ease of deployment at body temperature and removal, their thermo-mechanical properties can also be tailor made to meet the demands of a specific application (Lendlein & Langer, 2002; Lendlein et al., 2010; Serrano & Ameer, 2012; Srivastava et al., 2010; Wache et al., 2003). SMPs have the ability to sense external stimuli and move to their permanent shape thus releasing their stored entropic energy; actuators use this recovery force as a motor. Some other patents in relation to SMPs application are, intravascular delivery system, grippers, tunable automobile brackets in vehicles, dialysis needle adapter (Behl et al., 2009a; Heuchel et al., 2013; Lendlein et al., 2001; Lendlein et al., 2010; Mather et al., 2009; Ward Small et al., 2010). Shape memory effect also occurs on the microscopic level and as such SMPs have potential MEMS applications, micro/nano patterning, etc. (Lendlein et al., 2010; Leng et al., 2011; Mather et al., 2009; Sisson & Lendlein, 2012; Sun et al., 2012; Wache et al., 2003; Xie, 2011; Yakacki et al., 2011; Zhao, Behl, & Lendlein, 2013; Zotzmann, Behl, & Lendlein, 2011) .

Dual shape SMPs have the ability to remember one shape and can store one temporary shape, whereas TSMPs have the capability to remember three distinct shapes when stimulated by external triggers such as heat. In crystallizable TSMPs the formation of two distinct crystalline phases at different temperatures is used to fix two temporary shapes (Behl & Lendlein, 2012; Behl et al., 2009a; Behl et al., 2009b; Bellin et al., 2006; Heuchel et al., 2013; Lendlein et al., 2001; Mather et al., 2009; Sisson & Lendlein, 2012; Xie, 2011; Zhao et al., 2013; Zotzmann et al., 2011; Zotzmann et al., 2010a; Zotzmann et al., 2010b). The polymer returns from the second temporary shape to the first temporary shape and from there to the permanent shape due to the melting of the crystalline phases caused by heating. The mechanisms responsible for the shape-memory effect in crystallizable TSMPs i.e. the memory of the permanent shape and the formation of the temporary shapes are: the entanglement of polymer molecules, cross-linking, and material immobilization due to formation of a crystalline phase (see Irie, 1998, Kim et al., 2000, Lin & Chen, 1999). In this work we will focus on TSMPs.

In their rubbery state, polymer networks consist of flexible cross-linked polymer chains which, during deformation are oriented from a coiled state. The original shape is recovered as the polymer regains the entropy that was lost during orientation of the chains. The permanent shape of the polymer is primarily defined by its chemical cross-links or covalent net points during synthesis. Crystallizable TSMPs consist of two types of switching domains or crystallizable segments. Both of the switching domains have an individual transition temperature associated with them. In such polymers, the transition temperature is related to the thermal transition of the switching domains, which can be varied by altering the molecular structure of the polymer. One of the constituent domains, say phase-1 or P1, is chosen to have a higher transition temperature which we denote by θ_{r_1} (for recovery temperature), while the other domain, represented by phase-2 or P2, has a lower transition temperature, denoted by θ_{r_2} (for recovery temperature). At a temperature θ_H, which is above both the recovery temperatures ($\theta_{r_2} < \theta_{r_1} < \theta_H$), the polymer is in its permanent shape, returning to its original shape even after undergoing large deformations. In a process called as programming, typically a heating-deformation-cooling process, the polymer is deformed at θ_H and cooled while it is maintained in this deformed configuration. On cooling the polymer below θ_{r_1}, domain P1 partially crystallizes in the deformed configuration. These newly formed crystallites act as temporary cross-links which prevent the shape memory polymer from returning to its original shape. This leads to the fixation of the first temporary shape (B). On unloading the polymer below θ_{r_1}, a small amount of recovery is observed as the polymer has its original cross-links still in place. At a temperature θ_M, which is lower than the first recovery temperature but higher than the second recovery temperature ($\theta_{r_2} < \theta_M < \theta_{r_1} < \theta_H$), the polymer is deformed again. On cooling the polymer below θ_{r_2}, domain P2 partially crystallizes while domain P1 continues to crystallize, if the material is cooled while it is held in a deformed configuration, domain P2 and some part of domain P1 crystallize in the deformed configuration. These newly formed crystallites act as temporary crosslinks which prevent the polymer from going back to the first temporary shape (B). This leads to the fixation of the second temporary shape (A). On unloading the specimen at temperature θ_L, below the second transition temperature ($\theta_L < \theta_{r_2} < \theta_M < \theta_{r_1} < \theta_H$), a small amount of recovery is observed as the polymer has its original cross-links, and temporary cross-links formed during the crystallization of the first domain still in place. On subsequent heating above the second recovery temperature θ_{r_2}, the crystalline phase associated with the domain P2 melts and the polymer returns to its first temporary shape (B). On further heating above the first recovery temperature θ_{r_1}, the crystalline phase associated with the domain P1 melts and the shape memory polymer returns to its original shape (C). The orientation of the crystals formed below the two transition temperatures θ_{r_1} and θ_{r_2} depends on the deformation undergone by the polymer just prior to cooling (see Wang & Zhang, 1999). These crystals will have a preferred direction depending on the deformation that will cause the material properties to be anisotropic.

The triple shape memory behavior is illustrated schematically in Fig. 1 along with a typical uniaxial stress strain curve, Fig. 2. In Fig. 1, the filled circles represent the crosslinks (they could be chemical cross-links or hard domains), the wavy line

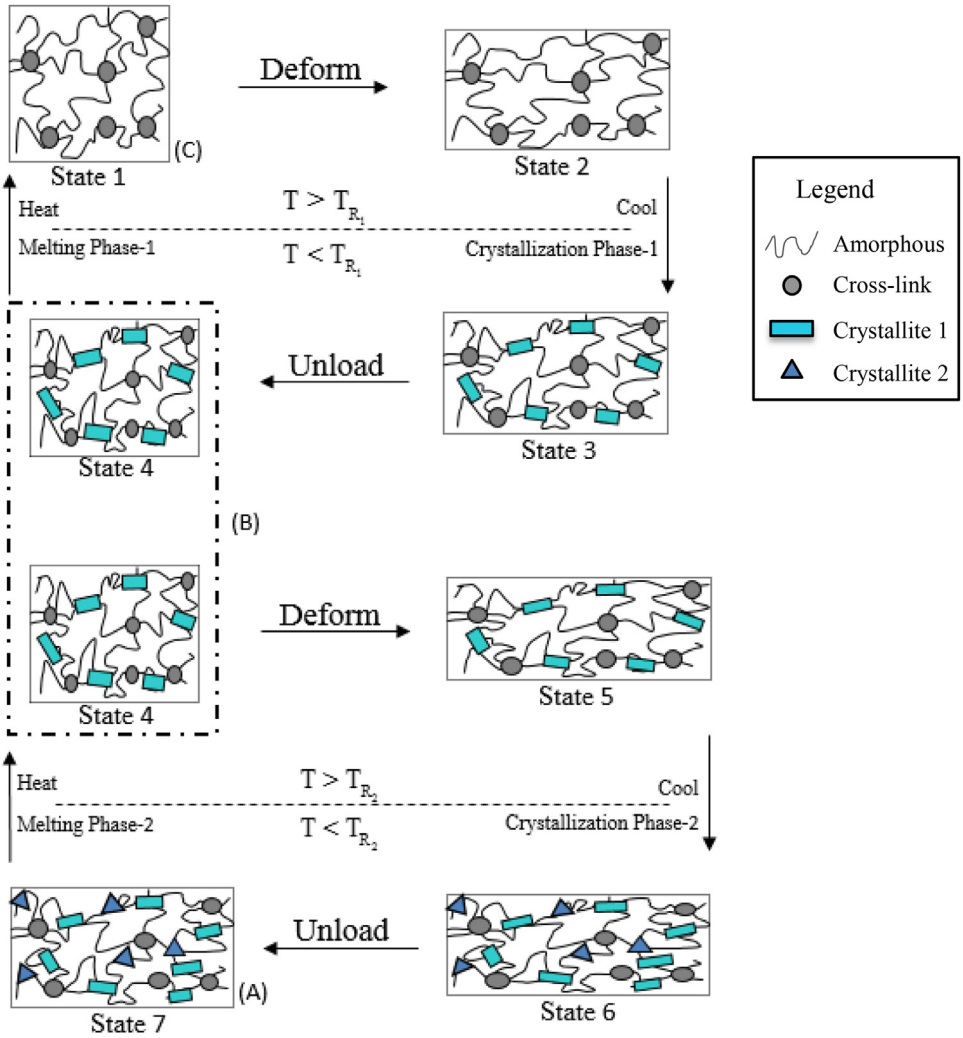

Fig. 1. Schematic illustration of the shape memory effect in triple shape memory polymers.

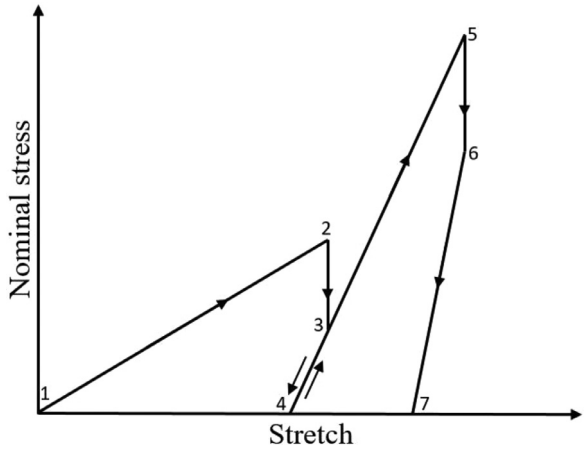

Fig. 2. A Typical nominal stress vs. stretch curve of a TSMP.

connecting the cross-links represents the crystallizable polymer in its amorphous state. The rectangular blocks represent the crystallizable domain, phase-1 or P1, in its crystalline state while the triangular blocks represent the crystallizable domain, phase-2 or P2, in its crystalline state. State-1 in both figures denotes the undeformed configuration. At a temperature θ_H above the recovery temperatures of both the domains, the polymer behavior is rubber-like and its elastic behavior is driven by changes in entropy. On deforming at this temperature the polymer molecules between the cross-links stretch (state-2). If the polymer is cooled to a temperature below the first recovery temperature θ_{r_1}, crystallization of the domain P1 (phase-1) takes place and the crystals are formed in this deformed configuration. The onset of crystallization is accompanied by a sharp drop in stress (from state 2 to state 3). After unloading (state 3 to state 4) the polymer remains in a deformed configuration with a small amount of recovery. This recovery is due to the presence of two components (amorphous and crystallites of domain P1 (phase-1)) each having their own stress free states. The amorphous part has a tendency to retract to its original configuration while the crystalline part prefers the deformed configuration. As the crystalline part is a lot stiffer, the recovery strain is small (see Fig. 2). At a temperature θ_M which is above the recovery temperature of the of the second domain P2 (phase-2) ($\theta_{r_2} < \theta_M < \theta_{r_1}$) the polymer is much stiffer as compared to stage 1, due to the presence of crystallites of domain P1. On deforming at this temperature the polymer molecules between the existing cross-links are stretched (state-5). If the polymer is cooled to a temperature below the second recovery temperature θ_{r_2}, crystallization of the domain P2 takes place and domain P1 continues to crystallize. The crystals are formed in the deformed configuration. The onset of crystallization is again accompanied by a sharp drop in stress (from state-5 to state-6). After unloading (state-6 to state-7) the polymer remains in a deformed configuration with a small amount of recovery. This recovery is due to the presence of three components; amorphous, crystallites of domain P1 and crystallites of domain P2, each having their own stress free states. The amorphous part, as mentioned earlier has a tendency to retract to its original configuration while the crystalline parts have a tendency to retract to the configuration when the crystallites were formed. Again, as the crystalline parts are a lot stiffer, the recovery strain is small (see Fig. 2). The mechanical response of the polymer in the semi-crystalline states below the recovery temperatures is similar to that of a semi-crystalline polymer with oriented crystallites, i.e., it is relatively stiff and the mechanical response is anisotropic. When the polymer is heated to above the second recovery temperature θ_{r_2} (from state-7 to state-4), the crystallites associated with the second domain P2 melt and the polymer retracts to the first temporary shape. On further heating above the first recovery temperature θ_{r_1}, the crystallites associated with the first domain P1 melt and the polymer retracts to its original shape.

As we can see from the above discussion, in order to model the thermo-mechanical behavior of triple shape memory polymers we need to characterize the processes of crystallization and transition of the two phases; as well as the behavior of the material both above and below the two recovery temperatures. At a temperature above both the transition temperatures the polymer behaves like rubber. When cooled to below their respective crystallization temperatures, both the domains i.e. the crystallizable part of the polymer crystallize. Behavior of the semi-crystalline phases is also like an anisotropic solid, for the range of deformations involved. These eight aspects of the modeling process are represented schematically in Fig. 1. In order to model the behavior of these materials undergoing complex deformations at different temperatures, it is important to have a fully three-dimensional model that satisfies all the physical requirements such as frame-indifference (or that of Galilean invariance), the requirements of the appropriate material symmetry, the second law of thermodynamics and other appropriate constraints. A possible fully thermodynamic framework within which to place the modeling under question is available and we plan to use this framework in this study.

Significant effort in the thermo-mechanical constitutive modeling of amorphous SMPs has been published in the literature (Anand et al., 2010; Boatti, Scalet, & Auricchio, 2016; Ge et al., 2012; Li, He, & Liu, 2017; Srivastava et al., 2010; Xiao & Nguyen, 2015; Xiao et al., 2015; Yu et al., 2012). In this paper we model the shape memory behavior in crystallizable triple shape memory polymers within a full thermo-mechanical setting that is able to incorporate the behavior of such bodies that have been observed to have different response characteristics in different regimes. In order to develop the model we will build upon earlier work concerning the general thermodynamic framework (see Rajagopal & Srinivasa, 2000, Rajagopal & Tao, 1995, Rao & Rajagopal, 2002) and shape memory polymers (see Barot, Rao, & Rajagopal, 2008). The model is formulated using the framework of multiple natural configurations that was introduced specifically for dissipative systems (see Rajagopal, 1995). This approach has been used to explain the material response of a large class of materials under unifying framework: multi-network theory (Rajagopal & Wineman, 1992), twinning (Rajagopal & Srinivasa, 1995), traditional plasticity (Rajagopal & Srinivasa, 1998), solid to solid phase transitions (Rajagopal & Srinivasa, 1999) and viscoelastic materials (Cui, Moon, & Rao, 2016; Rajagopal & Srinivasa, 2000; Rao & Rajagopal, 2007) have all been modeled within this framework, and classical elasticity and classical linearly viscous fluids arise naturally as sub-cases. Furthermore, the problem of crystallization of polymers and its application to film-blowing and fiber-spinning (Kannan & Rajagopal, 2005) have been investigated extensively. In addition to developing a general thermodynamic theory for crystallization (see Kannan, Rao, & Rajagopal, 2002, Kannan, Rao, & Rajagopal, 2006, Rao & Rajagopal, 2002, Rao & Rajagopal, 2000, Rao & Rajagopal, 2004, Rao & Rajagopal, 2005) it has been able to describe several applications with considerable success. Crystallizable dual shape memory polymers (Cui, Moon, & Joga Rao, 2017; Westbrook et al., 2010) and light activated shape memory polymers (Hamel, Cui, & Chester, 2017; Sodhi & Rao, 2010; Yuan, Muliana, & Rajagopal, 2017, Zhi) have also been modeled using this framework. In constitutive modeling literature many groups have developed frameworks that use the concept of phase evolution several examples include: soft active materials with phase evolution (Long, Dunn, & Jerry Qi, 2010), thermodynamics of photochemical reacting polymers (Long, Qi, & Dunn, 2013), thermally activated transitions in liquid crystal elastomers (Mitchell, Davis, & Guo, 1993), plastic deformation in shape memory alloys (Wang, Xu, & Yue, 2008), just to name a few.

In this paper we present a methodology for deriving the constitutive equations for the triple shape memory polymer in its amorphous as well as semi-crystalline states, the transition and the equations for the rate of crystallization and transition for both the phases using the above mentioned framework. The constitutive relations for stress, the crystallization kinetics, etc., are completely determined by the internal energy, entropy and rate of dissipation of each phase, conduction etc. These quantities in general depend on the temperature, mass fraction of the crystalline phase and kinematic variables, which are measured from an appropriate "natural configuration" which evolves as the body undergoes a process. The forms chosen for the constitutive equations are ones that are sufficient to satisfy the second law (Rao & Rajagopal, 2002; Rao & Rajagopal, 2004). We look for sufficient conditions as we are interested in the simplest forms that can model the observed phenomenon. We have assumed a general constitutive form for the rate of entropy production (see (Green & Naghdi, 1977; Rajagopal & Srinivasa, 2000; Truesdell, 1957) for a discussion of the rational for such an approach). The second law merely requires that the rate of entropy productions that are sought will satisfy it. In order to narrow this class and pick a rate of entropy production suited for the problem at hand we require that the rate of entropy production belonging to the class of rate of entropy productions that are sought will satisfy it, and we also require that the rate of entropy production be maximal amongst the set of functions that are non-negative. Evolution equations for the natural configuration and mass fraction of the crystalline material are obtained by maximizing the prescribed rate of entropy production and they are no ad hoc prescriptions. For triple shape memory polymers, it should be noted that both the amorphous and semi-crystalline phases are elastic, however the phase change process from one to the other is dissipative. We prescribe a rate of entropy production for both the crystallization and the transition process and show that the rate of crystallization, i.e., the crystallization kinetics, can be obtained directly from the fact that in an entropy producing process the rate of entropy production is maximized. To illustrate the application of the model that we have developed we solve for a typical uni-axial cycle of deformation and compare the results with experimental data. We have also solved a typical boundary value problem, the inflation and extension of a hollow cylinder with temperature variation. This is an inhomogeneous deformation and for this case we study two sub-cases, namely, crystallization under constant deformation and crystallization under constant pressure.

The remainder of this paper is organized as follows. In the next section we present the continuum framework and governing equations for TSMPs. This is followed by the application of the model to the problem of inflation and extension of a hollow cylinder. We conclude the paper with a discussion of the results and a summary of the paper.

Section 2. : Constitutive modeling

2.1. Overall model

As explained previously a typical triple shape cycle comprises of eight different processes: loading-1, cooling/crystallization-1, unloading-1, loading-2, cooling/crystallization-2, unloading-2, heating-1/ transition-1 and heating-2 /transition-2 i.e. return back to the amorphous phase (these transitions are usually referred to as melting but we prefer to refer to them as transition to the amorphous phase). The TSMP undergoes morphological changes during each of the processes. It is important to include these changes in the model. A continuum model is constructed here for the TSMP; which is applicable during the various processes undergone by the material, through the thermo-mechanical deformation cycle.

2.1.1. Isotropic rubbery phase

Behavior of the crystallizable triple shape memory polymers (TSMPs) above the recovery temperature is like isotropic rubber. Depending on the type of polymer the hard blocks or crosslinks act as connecting points. At a temperature above the transition temperatures these connecting points are responsible for remembering the original shape (C). The connecting points are linked by a network of flexible amorphous chain segments. The network will be elastic in nature if the temperature is above the transition temperature. Stretching these segments leads to a reduction in entropy. Upon removal of the load, the material returns to its original shape with a consequent increase in entropy. This type of behavior is well understood and is modeled as an incompressible hyper-elastic material. The triple shape memory polymer, at a temperature θ_{H}, above both the recovery temperatures ($\theta_{\mathrm{L}}<\theta_{\mathrm{r}_2}<\theta_{\mathrm{M}}<\theta_{\mathrm{r}_1}<\theta_{\mathrm{H}}$), is modeled as a hyper-elastic incompressible isotropic solid. For an incompressible isotropic elastic material the internal energy, entropy and Helmholtz potential are functions of temperature and the right Cauchy-Green stretch tensor C_{κ_a} through the first two invariants:

$$\varepsilon_a = \varepsilon_a(\theta, I_{C_a}, II_{C_a}), \tag{1.1}$$

$$\eta_a = \eta_a(\theta, I_{C_a}, II_{C_a}), \tag{1.2}$$

$$\psi_a = \psi_a(\theta, I_{C_a}, II_{C_a}), \tag{1.3}$$

Where the invariants are given by:

$$I_{B_a} = I_{C_a} = tr(B_{\kappa_a}) = tr(C_{\kappa_a}), II_{B_a} = II_{C_a} = tr(B^2{}_{\kappa_a}) = tr(C^2{}_{\kappa_a}). \tag{1.4}$$

Based on the Helmholtz potential (1.3) we assumed, and noting that there is no dissipation in the amorphous phase η_a we obtain:

$$\left(T - 2\rho\left[F_{\kappa_a}\frac{\partial\psi_a}{\partial C_{\kappa_a}}F^{\mathrm{T}}{}_{\kappa_a}\right]\right)\cdot D - \rho\left(\frac{\partial\psi_a}{\partial\theta} + \eta_a\right)\dot{\theta} = \zeta_d = 0. \tag{1.5}$$

Hence, for this material the Cauchy stress T is given by:

$$T = -pI + 2\rho\left[F_{\kappa_a}\frac{\partial\psi_a}{\partial C_{\kappa_a}}F^{\mathrm{T}}{}_{\kappa_a}\right] = -pI + 2\rho\left(\frac{\partial\psi_a}{\partial I_{B_a}}B_{\kappa_a} + 2\frac{\partial\psi_a}{\partial II_{B_a}}B^2{}_{\kappa_a}\right), \tag{1.6}$$

Where p is the indeterminate part of the stress due to the constraints of incompressibility and the Helmholtz potential is related to the entropy, through the following equation:

$$\frac{\partial\psi_a}{\partial\theta} = -\eta_a. \tag{1.7}$$

Also, Eq. (1.7) is equivalent to the following relation between the internal energy and entropy:

$$\frac{\partial\varepsilon_a}{\partial\theta} = \theta\frac{\partial\eta_a}{\partial\theta}. \tag{1.8}$$

Deformation influences internal energy in rubber like materials more than the temperature. By picking forms for the internal energy and entropy consistent with experimental results, specific models can be chosen to describe the behavior of the rubbery phase of the triple shape memory polymers. Here we have chosen the simplest hyper-elastic model, the neo-Hookean model, which often serves as a prototype for rubber-like materials (for details see Barot & Rao, 2006, Barot et al., 2008). For a neo-Hookean model with entropic-elasticity the internal energy and entropy are given by:

$$\varepsilon_a = C_a\theta + A_a,\ \eta_a = C_a\ln(\theta) + B_a\bar{\mu}_a(I_{B_a} - 3) \tag{1.9}$$

where, C_a is the specific heat of the amorphous phase, A_a and B_a are constants and $\bar{\mu}_a$ is the constant related to the shear modulus of the amorphous phase. Because of the chosen forms for the internal energy and the entropy, the Helmholtz potential is now just a function of the temperature and the first invariant of the stretch tensor only, and so Eq. (1.3) reduces to:

$$\psi_a = \psi_a(\theta, I_{B_a}) = \varepsilon_a - \theta\eta_a. \tag{1.10}$$

Substituting Eq. (1.10) into Eq. (1.6) we obtain the stress as:

$$T = -pI + \mu_a B_{\kappa_a}, \tag{1.11}$$

where, $\mu_a(= 2\rho\theta x\bar{\mu}_a)$ is the shear modulus of the amorphous region.

2.1.2. Phase transitions-I: amorphous phase to semi-crystalline phase (crystallization of phase-1)

On cooling below the first recovery temperature (θ_{r_1}) crystallization of phase-1 begins in the TSMP. One can find both the amorphous phase and the crystalline phase at the same time during the phase transition. We consider this mixture of phases as a constrained mixture. We allow co-occupancy of the phases at the same point, in a homogenized sense, as in traditional mixture theory (see Atkin & Craine, 1976, Bowen, 1976, Rajagopal & Tao, 1995). For details of using this approach see Rao & Rajagopal (2002) and Rao & Rajagopal (2000). The crystalline material of phase-1 that is newly formed is also an elastic solid. By finding the deformation gradient from a configuration of known stress to the current configuration, the stress in the current configuration can be calculated. In this case, the configuration of the deformed amorphous solid at the instant when the crystal is formed is assumed to be the stress free state of the newly born crystal. Such an assumption has proved to be successful in modeling polymer crystallization (see Rao & Rajagopal, 2002). As the material further deforms, this newly formed crystalline phase also undergoes deformation. The crystals that are formed afterwards are also born in their natural configurations, as described above. This temporary phase can be thought of as a mixture of an amorphous phase and a crystalline phase with different natural configurations. The configuration of the body at some time t is the natural configuration of the crystalline solid fraction born at the time$t$.

If crystallization of phase-1 at higher temperature begins at time t_{s_1} (see Fig. 3), and let τ be some time later than t_{s_1} and t the current time, i.e. $t_{s_1} < \tau < t$. For such a material the current internal energy (i.e., the internal energy at time t), entropy and the Helmholtz potential associated with the crystalline phase-1 formed at τ are given by (for a detailed discussion for the choice of the state variables on which the constitutive response functions depend on, see (Rao & Rajagopal, 2002)):

$$\varepsilon_{c_1} = \varepsilon_{c_1}(\theta, C_{\kappa_{c_1(\tau)}}), \tag{1.12}$$

$$\eta_{c_1} = \eta_{c_1}(\theta, C_{\kappa_{c_1(\tau)}}), \tag{1.13}$$

$$\psi_{c_1} = \psi_{c_1}(\theta, C_{\kappa_{c_1(\tau)}}). \tag{1.14}$$

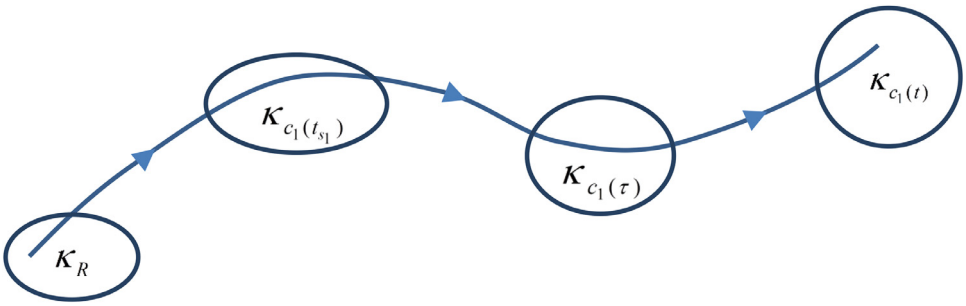

Fig. 3. The figure shows the evolution of the natural configurations during crystallization. At time t_{s_1}, crystallization of phase-1 begins. Between this time and current time t newly formed crystals are created in different configurations.

The internal energy and entropy of the mixture are assumed to be additive and can be given by:

$$\varepsilon = i_\varepsilon + (1-\alpha_1)\varepsilon_a + \int_{t_{s_1}}^{t} \varepsilon_{c_1} \frac{d\alpha_1}{d\tau} d\tau, \tag{1.15}$$

$$\eta = i_\eta + (1-\alpha_1)\eta_a + \int_{t_{s_1}}^{t} \eta_{c_1} \frac{d\alpha_1}{d\tau} d\tau, \tag{1.16}$$

where, α_1 is the crystallinity of phase-1, i_ε is the interfacial energy per unit mass of the amorphous-crystalline phase-1 mixture and i_η is the interfacial entropy per unit mass of the amorphous-crystalline phase-1 mixture. These interfacial components are added to account for the presence of phase boundaries. This is due to the fact that their presence will change the structure of the amorphous and crystalline regions in the vicinity of the interface. Also, ε_a and η_a are assumed to have the same form as that for the amorphous phase and are given by Eqs. (1.1) and (1.2). Using Eqs. (1.15) and (1.16), the Helmholtz potential for the mixture is then given by

$$\psi = i_\psi + (1-\alpha_1)\psi_a + \int_{t_{s_1}}^{t} \psi_{c_1} \frac{d\alpha_1}{d\tau} d\tau. \tag{1.17}$$

The crystalline phase-1 is formed gradually and not instantaneously, this is accounted by the presence of the integral in the Eq. (1.17). The anisotropy in the crystalline solid depends on the orientation of the amorphous phase at the instant of crystallization. Information about this orientation is given by the tensors $B_{\kappa_{a(i)}}, i = t_{s_1} < \tau < t_{f_1}$. A detailed discussion of the relevant issues can be found in Rao & Rajagopal (2000). The crystalline phase-1 is assumed to be orthotropic at each instant with the direction of anisotropy given by the eigenvectors of $B_{\kappa_{a(i)}}$ namely $n_{\kappa_{c_1(\tau)}}$ and $m_{\kappa_{c_1(\tau)}}$. For an incompressible orthotropic elastic solid, the Helmholtz potential depends on the first two invariants of the right Cauchy-Green tensor, $C_{\kappa_{c_1(\tau)}}$ which we denote by $I_{c_{c_1}}$ and $II_{c_{c_1}}$ and the following scalars

$$J_1 = n_{\kappa_{c_1(\tau)}} \cdot C_{\kappa_{c_1(\tau)}} n_{\kappa_{c_1(\tau)}}, J_2 = n_{\kappa_{c_1(\tau)}} \cdot C^2{}_{\kappa_{c_1(\tau)}} n_{\kappa_{c_1(\tau)}}, \tag{1.18}$$

$$K_1 = m_{\kappa_{c_1(\tau)}} \cdot C_{\kappa_{c_1(\tau)}} m_{\kappa_{c_1(\tau)}}, K_2 = m_{\kappa_{c_1(\tau)}} \cdot C^2{}_{\kappa_{c_1(\tau)}} m_{\kappa_{c_1(\tau)}} \tag{1.19}$$

The Helmholtz potential for an incompressible orthotropic elastic solid can then be written as:

$$\psi_{c_1} = \psi_{c_1}(\theta, I_{c_{c_1}}, II_{c_{c_1}}, J_1, J_2, K_1, K_2), \tag{1.20}$$

where, the invariants depend on t and τ. Based on the Helmholtz potential for the mixture region (Eqs. (1.17), (1.3), (1.20)), and noting that the only source of dissipation is due to phase change we obtain:

$$\begin{aligned} &\left(T - (1-\alpha_1)2\rho\left[F_{\kappa_a}\frac{\partial\psi_a}{\partial C_{\kappa_a}}F^{\mathrm{T}}{}_{\kappa_a}\right] - 2\rho\left[\int_{t_{s_1}}^{t} F_{\kappa_{c_1(\tau)}}\frac{\partial\psi_{c_1}}{\partial C_{\kappa_{c_1(\tau)}}}F_{\kappa_{c_1(\tau)}}\frac{d\alpha_1}{d\tau}d\tau\right]\right)\cdot D \\ &-\rho\left(\frac{\partial\psi}{\partial\theta}+\eta\right)\dot{\theta} + \rho\left(\psi_a - \psi_{c_1}|_{C_{\kappa_{c_1(\tau)}}=I} - \frac{\partial i_\psi}{\partial\alpha_1}\right)\dot{\alpha}_1 = \zeta_p \geq 0. \end{aligned} \tag{1.21}$$

It follows that sufficient condition that will satisfy the above inequality is a general form for the stress given by:

$$T = -pI + 2(1-\alpha_1)\rho\left[\frac{\partial\psi_a}{\partial I_B}B_{\kappa_a} + 2\frac{\partial\psi_a}{\partial II_B}B^2{}_{\kappa_a}\right] + 2\rho\left[\int_{t_{s_1}}^{t} F_{\kappa_{c_1(\tau)}}\frac{\partial\psi_{c_1}}{\partial C_{\kappa_{c_1(\tau)}}}F_{\kappa_{c_1(\tau)}}\frac{d\alpha_1}{d\tau}d\tau\right] \tag{1.22}$$

The entropy and the Helmholtz potential are re lated through

$$\frac{\partial\psi}{\partial\theta} = -\eta \tag{1.23}$$

and

$$\rho\left(\psi_a - \psi_{c_1}|_{C_{\kappa_{c_1}(\tau)}=I} - \frac{\partial i_\psi}{\partial \alpha_1}\right)\dot{\alpha}_1 = \zeta_p \geq 0 \tag{1.24}$$

Eq. (1.24) is used for prescribing both the activation criterion and the crystallization rate for the first crystalline phase i.e. phase-1. The term inside the bracket of Eq. (1.24) is the difference between the Helmholtz potentials of the amorphous phase and crystalline phase-1 and acts as the driving force D_{f_1} for crystallization of phase-1. It can be defined as:

$$D_{f_1} = \left(\psi_a - \psi_{c_1}\Big|_{C_{\kappa_{c_1}(\tau)}=I} - \frac{\partial i_\psi}{\partial \alpha_1}\right) \tag{1.25}$$

The crystallinity of phase-1 is identically zero when the crystallization is initiated, and the driving force is given by

$$D_{f_1}|_{\alpha_1=0} := \left(\psi_a - \psi_{c_1}\Big|_{C_{\kappa_{c_1}(\tau)}=I} - \frac{\partial i_\psi}{\partial \alpha_1}|_{\alpha_1=0}\right). \tag{1.26}$$

The driving force can be used to define the activation function for crystalline phase-1 as

$$\phi_1(\theta, B_{\kappa_a}) = D_{f_1}|_{\alpha_1=0} - A_1, \tag{1.27}$$

where, A_1 is the initiation barrier for crystalline phase-1 and is a positive constant. The crystalline material of phase-1 is formed in a stress free state and hence the activation criterion depends on the temperature θ and tensor B_{κ_a}. If the following conditions are met crystallization of phase-1 commences:

$$\phi_1(\theta, B_{\kappa_a}) > 0 \tag{1.28a}$$

or

$$\phi_1(\theta, B_{\kappa_a}) = 0, \quad \text{and} \quad \frac{\partial \phi_1}{\partial \theta}\dot{\theta} + \frac{\partial \phi_1}{\partial B_{\kappa_a}}\dot{B}_{\kappa_a} > 0. \tag{1.28b}$$

Using Eq. (1.25), Eq. (1.24) can be re-written as follows:

$$\rho D_{f_1}\dot{\alpha}_1 = \zeta_p = \zeta_{p_1}. \tag{1.29}$$

As the second phase is not crystallizing at this point, rate of dissipation due to crystallization of second phase, ζ_{p_2} is zero. By prescribing a form for the rate of dissipation associated with crystallization of phase-1, i.e., ζ_{p_1} the crystallization rate for phase-1 can be obtained by using Eq. (1.29). More than one value of $\dot{\alpha}_1$ is possible, as Eq. (1.29) is in general non-linear. The value of $\dot{\alpha}_1$ that maximizes the rate of dissipation is the one that is chosen. Hence, it is necessary to prescribe the rate of dissipation, to derive the rate of crystallization of phase-1. It is assumed that ζ_{p_1} depends on the crystallinity of phase-1, α_1, crystallization rate of phase-1, $\dot{\alpha}_1$ and temperature, θ. It can also depend on the other kinematical variables, i.e.

$$\zeta_{p_1} = \zeta_{p_1}(\alpha_1, \dot{\alpha}_1, \theta, \ldots) \geq 0. \tag{1.30}$$

Note that the rate of dissipation due to crystallization of phase-1 ζ_{p_1}, is exactly zero when no crystallization is taking place i.e.

$$\zeta_{p_1}\Big|_{\dot{\alpha}_1=0} = 0. \tag{1.31}$$

Specific forms used in this work for crystalline phase-1 and the rate of dissipation associated with it are discussed next. The configurational entropy does not change significantly with the deformation for crystalline materials; however, the internal energy depends on the deformation. With this in mind we use the following forms for the internal energy and the entropy of crystalline phase-1:

$$\varepsilon_{c_1} = C_{c_1} + A_{c_1} + \frac{1}{2\rho}(\mu_{c_1}(I_{c_{c_1}} - 3) + \mu_{c_1 1}(J_1 - 1)^2 + \mu_{c_1 2}(K_1 - 1)^2), \tag{1.32}$$

$$\eta_{c_1} = C_{c_1}\ln(\theta) + B_{c_1}, \tag{1.33}$$

$$\psi_{c_1} = C_{c_1}\theta + A_{c_1} + \frac{1}{2\rho}(\mu_{c_1}(I_{c_{c_1}} - 3) + \mu_{c_1 1}(J_2 - 1)^2 + \mu_{c_1 2}(K_2 - 1)^2) - C_{c_1}\ln(\theta) + B_{c_1}, \tag{1.34}$$

where, C_{c_1} is the specific heat associated with the crystalline phase-1, A_{c_1} and B_{c_1} are constants an $\mu_{c_1}, \mu_{c_1 1}$ and $\mu_{c_1 2}$ are the material moduli associated with crystalline phase-1. Note the above forms automatically satisfy Eq. (1.23). For this choice of stored energy, using Eqs. (1.10) and (1.20) in Eq. (1.22) the total stress is obtained as:

$$\begin{aligned} T = &-pI + (1-\alpha_1)\mu_a B_{\kappa_a} + \int_{t_{s_1}}^{t} \mu_{c_1 1} B_{\kappa_{c_1(\tau)}} \frac{d\alpha_1}{d\tau} d\tau + \int_{t_{s_1}}^{t} (F_{\kappa_{c_1(\tau)}}(\mu_{c_1 1}(J_1 - 1) n_{\kappa_{c_1(\tau)}} \otimes n_{\kappa_{c_1(\tau)}} \\ &+ \mu_{c_1 2}(K_1 - 1) m_{\kappa_{c_1(\tau)}} \otimes m_{\kappa_{c_1(\tau)}}) F^{\mathrm{T}}{}_{\kappa_{c_1(\tau)}}) \frac{d\alpha_1}{d\tau} d\tau. \end{aligned} \tag{1.35}$$

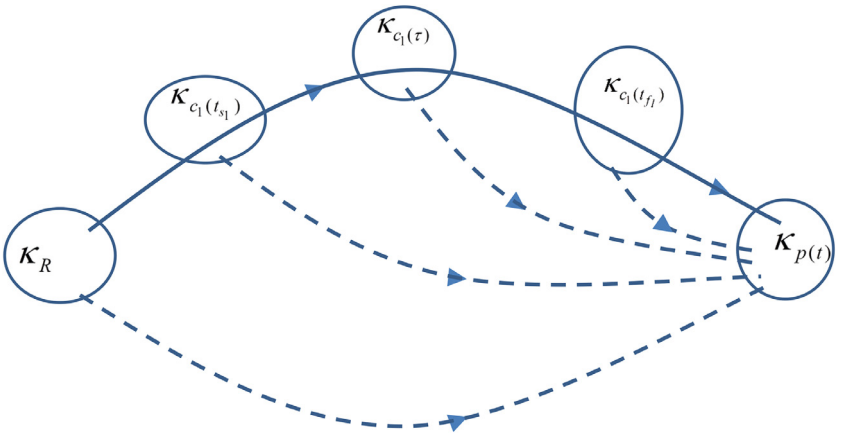

Fig. 4. The figure shows the evolution of the natural configurations during unloading (to the configuration $\kappa_{p(t)}$) after the first crystallization ($t_{s_1} < t < t_{f_1}$).

The energy equation is derived by using the law of conservation of energy, resulting in:

$$\rho((1-\alpha_1)C_a + \alpha_1 C_{c_1})\dot{\theta} + \mathrm{div} q = (1-\alpha_1)\mu_a B_{\kappa_a}\cdot L + \rho\left(C_a\theta + A_a - C_{c_1}\theta - A_{c_1} - \frac{\partial i_\psi}{\partial \alpha_1}\right)\dot{\alpha}_1 + \rho r \tag{1.36}$$

Using the specific forms chosen for the thermodynamic quantities for the amorphous and crystalline phase-1 in this work, the activation function for crystallization of phase-1 reduces to:

$$\phi(\theta, B_{\kappa_a}) = \left(\frac{\theta_{r_1} - \theta}{\theta_{r_1}}\right) - \frac{1}{\Delta H_a}\frac{\partial i_\psi}{\partial \alpha_1}|_{\alpha_1=0} + \frac{\mu_a(I_{B_{\kappa_a}} - 3)}{2\rho\Delta H_a}, \tag{1.37}$$

where, ΔH_a is the latent heat (for details of the derivation see Rao & Rajagopal, 2002). In this work, for phase-1 the form chosen for the rate of dissipation associated with crystallization is:

$$\zeta_{p_1} = \frac{\dot{\alpha}_1^{m_1}}{\bar{G}_1(\alpha_{1_0} - \alpha_1)^{k_1}}, \tag{1.38}$$

where, the constant α_{1_0} represents the maximum crystallinity associated with phase-1 and $\bar{G}_1$, k_1 and m_1 are constants. For the chosen form of the rate of dissipation, as crystallinity of phase-1 reaches its maximum value, the rate of dissipation becomes very large, effectively curbing any further crystallization. This form also fulfills the required conditions as in Eq. (1.31). The crystallization rate for phase-1 for the chosen form of the rate of dissipation takes the following form:

$$\dot{\alpha}_1 = G_1(\alpha_{1_0} - \alpha_1)^{k_1/m_1 - 1}\left(\left(\frac{\theta_{r_1} - \theta}{\theta_{r_1}}\right) - \frac{1}{\Delta H_a}\frac{\partial i_\psi}{\partial \alpha_1} + \frac{\mu_a(I_{B_{\kappa_a}} - 3)}{2\rho\Delta H_a}\right)^{1/m_1 - 1} \tag{1.39}$$

where G_1 is a constant.

2.1.3. The semi-crystalline phase after crystallization of phase-1 at higher temperature

At a temperature θ_M which is below the higher recovery temperature (θ_{r_1}) and above the lower recovery temperature (θ_{r_2}) ($\theta_L < \theta_{r_2} < \theta_M < \theta_{r_1} < \theta_H$) crystallization of phase-1 at higher temperature ceases. The material is a mixture of amorphous phase and crystalline phase-1. The TSMP behaves like an anisotropic elastic material, the anisotropy is a consequence of the presence of crystalline phase-1. This material has multiple natural configurations associated with it, one for the amorphous phase and multiplicity of natural configurations for the crystalline phase-1. Note that if the crystallization takes place at a single configuration, the crystalline phase-1 will have only one natural configuration. As shown in Fig. 4, after the cessation of crystallization of phase-1, the Helmholtz potential in the material depends on the deformation gradients between the natural configurations and the current configuration. The Helmholtz potential for such a hyperelastic solid will be then given by

$$\psi = i_\psi + (1-\alpha_1)\psi_a + \int_{t_{s_1}}^{t_{f_1}} \psi_{c_1}\frac{d\alpha_1}{d\tau}d\tau. \tag{1.40}$$

Note that other than the change in the limits of integration, Eq. (1.40) is very similar to Eq. (1.17). This is due to the fact that the crystallization stops at a time t_{f_1} and the amorphous phase and the crystalline phase-1 are fixed. Hence, the Cauchy stress is similar to Eq. (1.35) with a change in the limits and is given by

$$\begin{aligned} T = &-pI + (1-\alpha_1)\mu_a B_{\kappa_a} + \int_{t_{s_1}}^{t_{f_1}} \mu_{c_1 1} B_{\kappa_{c_1(\tau)}}\frac{d\alpha_1}{d\tau}d\tau + \int_{t_{s_1}}^{t_{f_1}} (F_{\kappa_{c_1(\tau)}}(\mu_{c_1 1}(J_1 - 1)n_{\kappa_{c_1(\tau)}} \otimes n_{\kappa_{c_1(\tau)}} \\ &+\mu_{c_1 2}(K_1 - 1)m_{\kappa_{c_1(\tau)}} \otimes m_{\kappa_{c_1(\tau)}})F^{\mathrm{T}}{}_{\kappa_{c_1(\tau)}})\frac{d\alpha_1}{d\tau}d\tau. \end{aligned} \tag{1.41}$$

2.1.4. Amorphous phase to semi-crystalline phases (crystallization at lower temperature)

On cooling below the lower recovery temperature (θ_{r_2}), crystallization of the second crystalline phase i.e. phase-2 begins in the TSMP, the first crystalline phase i.e. phase-1 also continues to crystallize at the lower temperature. During this second cooling process, which is carried out at a lower temperature, one can find the amorphous phase and the two crystalline phases at the same time. As described earlier the stress in the current configuration can be calculated by finding the deformation gradient from a configuration of known stress, to the current configuration. This temporary phase can be thought of as a mixture of an amorphous phase, crystalline phase-1 and crystalline phase-2 with different natural configurations. Also as discussed earlier the natural configuration of the crystalline solid fraction of both the phases born at some time t is the configuration of the body at time t. If the crystallization at a lower temperature begins at time t_{s_2}, which is later than time t_{f_1} (see Fig. 4), and let τ be some time later than t_{s_2} and t the current time, i.e. $t_{s_1} < t_{f_1} < t_{s_2} < \tau < t$. For such a material the current internal energy (i.e., the internal energy at time t), entropy and the Helmholtz potential associated with the crystalline phase-2 formed at τ are given by (for a detailed discussion for the choice of the state variables on which the constitutive response depend on, see Barot et al., 2008 and Rao & Rajagopal, 2002).

$$\varepsilon_{c_2} = \varepsilon_{c_2}(\theta, C_{\kappa_{c_2(\tau)}}), \tag{1.42}$$

$$\eta_{c_2} = \eta_{c_2}(\theta, C_{\kappa_{c_2(\tau)}}), \tag{1.43}$$

$$\psi_{c_2} = \psi_{c_2}(\theta, C_{\kappa_{c_2(\tau)}}). \tag{1.44}$$

The current internal energy (i.e., the internal energy at time t), entropy and the Helmholtz potential associated with the crystalline phase-1 formed at lower temperature, at τ ($t_{s_1} < t_{f_1} < t_{s_2} < \tau < t$) are given by Eqs. (1.12), (1.13), (1.14), respectively with the only difference that τ is some time later than t_{s_2}. The internal energy (at time t), entropy and the Helmholtz potential associated with the crystalline phase-1 formed at the higher temperature, are the same as discussed earlier and are given by Eqs. (1.12), (1.13), (1.14) where τ is sometime between t_{s_1} and t_{f_1} when these crystallites were formed. The internal energy and the entropy of the mixture are assumed to be additive and are given by:

$$\varepsilon = i_\varepsilon + (1-\alpha_1-\alpha_2)\varepsilon_a + \int_{t_{s_1}}^{t} \varepsilon_{c_1}\frac{d\alpha_1}{d\tau}d\tau + \int_{t_{s_2}}^{t} \varepsilon_{c_2}\frac{d\alpha_2}{d\tau}d\tau, \tag{1.45}$$

$$\eta = i_\varepsilon + (1-\alpha_1-\alpha_2)\eta_a + \int_{t_{s_1}}^{t} \eta_{c_1}\frac{d\alpha_1}{d\tau}d\tau + \int_{t_{s_2}}^{t} \eta_{c_2}\frac{d\alpha_2}{d\tau}d\tau, \tag{1.46}$$

where, α_2 is the crystallinity of the second crystalline phase. The Helmholtz potential of the mixture is given by

$$\psi = i_\varepsilon + (1-\alpha_1-\alpha_2)\psi_a + \int_{t_{s_1}}^{t} \psi_{c_1}\frac{d\alpha_1}{d\tau}d\tau + \int_{t_{s_2}}^{t} \psi_{c_2}\frac{d\alpha_2}{d\tau}d\tau, \tag{1.47}$$

As discussed earlier, the presence of the integrals in the Eq. (1.47) is due to the fact that the crystalline phases are formed gradually and not instantaneously. As mentioned earlier, the anisotropy in the semi-crystalline phase depends on the orientation of the amorphous phase at the instant of crystallization. The tensors $B_{\kappa_{a(i)}}, i = t_{s_1} < \tau < t_{f_1} < t_{s_2} < \tau < t_{f_2}$, give us information about this orientation. The crystalline phases are again assumed to be orthotropic at each instant with the direction of anisotropy given by the eigenvectors of $B_{\kappa_{a(i)}}$, namely $n_{\kappa_{c_1(\tau)}}$, $m_{\kappa_{c_1(\tau)}}$, $n_{\kappa_{c_2(\tau)}}$ and $m_{\kappa_{c_2(\tau)}}$. For crystalline phase-2, the Helmholtz potential depends on the first two invariants of the Cauchy–Green tensor, $B_{\kappa_{c_2(\tau)}}$ which we denote by $I_{c_{c_2}}$, $II_{c_{c_2}}$ and the following scalars (see Spencer, 1972)

$$J_3 = n_{\kappa_{c_2(\tau)}} \cdot C_{\kappa_{c_2(\tau)}} n_{\kappa_{c_2(\tau)}}, J_4 = n_{\kappa_{c_2(\tau)}} \cdot C^2{}_{\kappa_{c_2(\tau)}} n_{\kappa_{c_2(\tau)}}, \tag{1.48}$$

$$K_3 = m_{\kappa_{c_2(\tau)}} \cdot C_{\kappa_{c_2(\tau)}} m_{\kappa_{c_2(\tau)}}, K_4 = m_{\kappa_{c_2(\tau)}} \cdot C^2{}_{\kappa_{c_2(\tau)}} m_{\kappa_{c_2(\tau)}}, \tag{1.49}$$

The Helmholtz potential for the crystalline phase-2 can be written as:

$$\psi_{c_2} = \psi_{c_2}(\theta, I_{c_{c_2}}, II_{c_{c_2}}, J_3, J_4, K_3, K_4) \tag{1.50}$$

Where the invariants depend upon t and τ. The Helmholtz potential for crystalline phase-1 that crystallizes at lower temperature below second recovery temperature is given by Eq. (1.20), with the difference that τ is a time between t_{s_2} and current time t. Based on the Helmholtz potential for the mixture region (Eqs (1.47), (1.50), (1.20) and (1.3)), and noting that the only source of dissipation is due to phase change we obtain:

$$\begin{aligned}&\left(T-(1-\alpha_1-\alpha_2)2\rho\left[F_{\kappa_a}\frac{\partial\psi_a}{\partial C_{\kappa_a}}F^{\mathrm{T}}{}_{\kappa_a}\right]-2\rho\left[\int_{t_{s_1}}^{t}F_{\kappa_{c_1(\tau)}}\frac{\partial\psi_{c_1}}{\partial C_{\kappa_{c_1(\tau)}}}F_{\kappa_{c_1(\tau)}}\frac{d\alpha_1}{d\tau}d\tau\right]\right.\\&\left.-2\rho\left[\int_{t_{s_2}}^{t}F_{\kappa_{c_2(\tau)}}\frac{\partial\psi_{c_2}}{\partial C_{\kappa_{c_2(\tau)}}}F_{\kappa_{c_2(\tau)}}\frac{d\alpha_2}{d\tau}d\tau\right]\right)\cdot D-\rho\left(\frac{\partial\psi}{\partial\theta}+\eta\right)\dot{\theta}\\&+\rho\left(\psi_a-\psi_{c_1}\Big|_{C_{\kappa_{c_1(\tau)}}=I}-\frac{\partial i_\psi}{\partial\alpha_1}\right)\dot{\alpha}_1+\rho\left(\psi_a-\psi_{c_2}\Big|_{C_{\kappa_{c_2(\tau)}}=I}-\frac{\partial i_\psi}{\partial\alpha_2}\right)\dot{\alpha}_2=\zeta_p=\zeta_{p_1}+\zeta_{p_2}\geq 0.\end{aligned}\tag{1.51}$$

It follows that the sufficient condition that will satisfy the above inequality is a general form for the stress given by:

$$\begin{aligned}T=&-pI+2(1-\alpha_1-\alpha_2)\rho\left[\frac{\partial\psi_a}{\partial I_B}B_{\kappa_a}+2\frac{\partial\psi_a}{\partial II_B}B^2{}_{\kappa_a}\right]+2\rho\left[\int_{t_{s_1}}^{t}F_{\kappa_{c_1(\tau)}}\frac{\partial\psi_{c_1}}{\partial C_{\kappa_{c_1(\tau)}}}F_{\kappa_{c_1(\tau)}}\frac{d\alpha_1}{d\tau}d\tau\right]\\&+2\rho\left[\int_{t_{s_2}}^{t}F_{\kappa_{c_2(\tau)}}\frac{\partial\psi_{c_2}}{\partial C_{\kappa_{c_2(\tau)}}}F_{\kappa_{c_2(\tau)}}\frac{d\alpha_2}{d\tau}d\tau\right]\end{aligned}\tag{1.52}$$

The entropy and the Helmholtz potential are related through

$$\frac{\partial\psi}{\partial\theta}=-\eta;\tag{1.53}$$

and

$$\rho\left(\psi_a-\psi_{c_1}\Big|_{C_{\kappa_{c_1(\tau)}}=I}-\frac{\partial i_\psi}{\partial\alpha_1}\right)\dot{\alpha}_1+\rho\left(\psi_a-\psi_{c_2}\Big|_{C_{\kappa_{c_2(\tau)}}=I}-\frac{\partial i_\psi}{\partial\alpha_2}\right)\dot{\alpha}_2=\zeta_p=\zeta_{p_1}+\zeta_{p_2}\geq 0\tag{1.54}$$

Note that we have split the rate of dissipation due to phase change into two different components for the two different phases, phase-1 and phase-2. ζ_{P_1} is the rate of dissipation associated with crystallization of phase-1 and ζ_{P_2} is the rate of dissipation associated with crystallization of phase-2.

$$\zeta_{P_1}=\rho\left(\psi_a-\psi_{c_1}\Big|_{C_{\kappa_{c_1(\tau)}}=I}-\frac{\partial i_\psi}{\partial\alpha_1}\right)\dot{\alpha}_1\tag{1.55}$$

$$\zeta_{P_2}=\rho\left(\psi_a-\psi_{c_2}\Big|_{C_{\kappa_{c_2(\tau)}}=I}-\frac{\partial i_\psi}{\partial\alpha_2}\right)\dot{\alpha}_2\tag{1.56}$$

Eq. (1.56) is used for both prescribing the activation criterion and the crystallization rate for crystalline phase-2. The activation criterion for phase-1 has already been prescribed. The term in the bracket for Eq. (1.56) is the difference between the Helmholtz potential of the amorphous phase and crystalline phase-2 and acts as the driving force D_{f_2} for the crystallization of phase-2. It can be defined as:

$$D_{f_2}:=\left(\psi_a-\psi_{c_2}|_{C_{\kappa_{c_2(\tau)}}=I}-\frac{\partial i_\psi}{\partial\alpha_2}\right).\tag{1.57}$$

When crystallization of phase-2 is initiated, its crystallinity is identically zero, and the driving force is given by

$$D_{f_2}|_{\alpha_2=0}:=\left(\psi_a-\psi_{c_2}\Big|_{C_{\kappa_{c_2(\tau)}}=I}-\frac{\partial i_\psi}{\partial\alpha_2}|_{\alpha_2=0}\right)\tag{1.58}$$

The activation function can be defined through the driving force as

$$\phi_2(\theta,B_{\kappa_a})=D_{f_2}|_{\alpha_2=0}-A_2\tag{1.59}$$

where, A_2 is the initiation barrier and is a positive constant. As the crystalline material is formed in a stress free state, the activation criterion depends on the temperature θ and tensor B_{κ_a}. Crystallization of phase-2 is initiated if the following conditions are met:

$$\phi_2(\theta,B_{\kappa_a})>0\tag{1.60a}$$

Or

$$\phi_2(\theta,B_{\kappa_a})=0,\quad\text{and}\quad\frac{\partial\phi_2}{\partial\theta}\dot{\theta}+\frac{\partial\phi_2}{\partial B_{\kappa_a}}\dot{B}_{\kappa_a}>0\tag{1.60b}$$

Using Eq. (1.57), Eq. (1.56) can be re-written as follows:

$$\rho D_{f_2}\dot{\alpha}_2=\zeta_{p_2}\tag{1.61}$$

The crystallization rate for phase-2 can be obtained from Eq. (1.61) by prescribing a form for the rate of dissipation associated with it, namelyζ_{p_2}. More than one value of $\dot{\alpha}_2$ is possible, as Eq. (1.61) is in general non-linear. The value of $\dot{\alpha}_2$ maximizing the rate of dissipation is chosen. It is assumed that ζ_{p_2} depends on the crystallinity of phase-2, α_2 crystallization rate of phase-2, $\dot{\alpha}_2$ and temperature θ. It can depend on the other kinematical variables, i.e.

$$\zeta_{p_2}=\zeta_{p_2}(\alpha_2,\dot{\alpha}_2,\theta,\ldots)\geq 0.\tag{1.62}$$

Note that when no crystallization of phase-2 is taking place, the rate of dissipation ζ_{p_2} is exactly zero, i.e.

$$\zeta_{p_2}\big|_{\dot{\alpha}_2=0} = 0. \tag{1.63}$$

This completes the general equations for the phase transition from the amorphous to semi-crystalline phase, which occur during the two cooling processes. The specific forms used in this work for the second crystalline phase and the rate of dissipation associated with it are discussed next.

Proceeding in a manner similar to phase-1, the following forms are used for the internal energy and the entropy in crystalline phase-2:

$$\varepsilon_{c_2} = C_{c_2} + A_{c_2} + \frac{1}{2\rho}(\mu_{c_2}(I_{c_{c_2}} - 3) + \mu_{c_21}(J_3 - 1)^2 + \mu_{c_22}(K_3 - 1)^2), \tag{1.64}$$

$$\eta_{c_2} = C_{c_2}\ln(\theta) + B_{c_2}, \tag{1.65}$$

$$\psi_{c_2} = C_{c_2}\theta + A_{c_2} + \frac{1}{2\rho}(\mu_{c_2}(I_{c_{c_2}} - 3) + \mu_{c_21}(J_3 - 1)^2 + \mu_{c_12}(K_3 - 1)^2) - C_{c_2}\ln(\theta) + B_{c_2}, \tag{1.66}$$

where, C_{c_2} is the specific heat associated with crystalline phase-2, A_{c_2} and B_{c_2} are constants and μ_{c_2}, μ_{c_21} and μ_{c_22} are the material moduli associated with crystalline phase-2. Note the above forms automatically satisfy Eq. (1.53). The forms for internal energy and entropy of phase-1 that crystallizes at lower temperature are similar to Eqs. (1.32)–(1.34) with the exception that τ is some intermediate time between t_{s_2} and current time t. For this choice of stored energy, using Eqs. (1.10) and (1.66) in Eq. (1.52) the total stress is obtained as:

$$\begin{aligned} T = &-pI + (1-\alpha_1-\alpha_2)\mu_a B_{\kappa_a} + \int_{t_{s_1}}^{t} \mu_{c_1} B_{\kappa_{c_1(\tau)}} \tfrac{d\alpha_1}{d\tau} d\tau + \int_{t_{s_1}}^{t} (F_{\kappa_{c_1(\tau)}}(\mu_{c_11}(J_1-1) n_{\kappa_{c_1(\tau)}} \otimes n_{\kappa_{c_1(\tau)}} \\ &+\mu_{c_12}(K_1-1) m_{\kappa_{c_1(\tau)}} \otimes m_{\kappa_{c_1(\tau)}}) F^{\mathrm{T}}{}_{\kappa_{c_1(\tau)}}) \tfrac{d\alpha_1}{d\tau} d\tau + \int_{t_{s_2}}^{t} \mu_{c_21} B_{\kappa_{c_2(\tau)}} \tfrac{d\alpha_2}{d\tau} d\tau_2 \\ &+ \int_{t_{s_2}}^{t} (F_{\kappa_{c_2(\tau)}}(\mu_{c_21}(J_3-1) n_{\kappa_{c_2(\tau)}} \otimes n_{\kappa_{c_2(\tau)}} + \mu_{c_22}(K_3-1) m_{\kappa_{c_2(\tau)}} \otimes m_{\kappa_{c_2(\tau)}}) F^{\mathrm{T}}{}_{\kappa_{c_2(\tau)}}) \tfrac{d\alpha_2}{d\tau} d\tau. \end{aligned} \tag{1.67}$$

With the law of conservation of energy, the energy equation for the mixture can be given as:

$$\begin{aligned} &\rho((1-\alpha_1-\alpha_2)C_a + \alpha_1 C_{c_1} + \alpha_2 C_{c_2})\dot{\theta} + \mathrm{div} q = (1-\alpha_1-\alpha_2)\mu_a B_{\kappa_a} \cdot L \\ &+\rho\left(C_a\theta + A_a - C_{c_1}\theta - A_{c_1} - \tfrac{\partial i_\psi}{\partial \alpha_1}\right)\dot{\alpha}_1 + \rho\left(C_a\theta + A_a - C_{c_2}\theta - A_{c_2} - \tfrac{\partial i_\psi}{\partial \alpha_2}\right)\dot{\alpha}_2 + \rho r. \end{aligned} \tag{1.68}$$

For the specific forms chosen for the thermodynamic quantities for the amorphous phase and crystalline phase-2 in this work, the activation function for crystallization of crystalline phase-2 reduces to:

$$\phi_2(\theta, B_{\kappa_a}) = \left(\frac{\theta_{r_2} - \theta}{\theta_{r_2}}\right) - \frac{1}{\Delta H_a}\frac{\partial i_\psi}{\partial \alpha_2}\Big|_{\alpha_2=0} + \frac{\mu_a(I_{B_{\kappa_a}} - 3)}{2\rho\Delta H_a}, \tag{1.69}$$

Where, ΔH_a is the latent heat (for details of the derivation see Barot et al., 2008 and Rao & Rajagopal, 2002). In this work, the form chosen for the rate of dissipation associated with crystallization of phase-2 is:

$$\zeta_{p_2} = \frac{\dot{\alpha}_2^{m_2}}{\bar{G}_2(\alpha_{2_0} - \alpha_2)^{k_2}}, \tag{1.70}$$

Where the constant α_{2_0} represents the maximum crystallinity of phase-2 and $\bar{G}_2$, k_2 and m_2 are constants. For the chosen form of rate of the dissipation of phase-2, as crystallinity of phase-2 reaches its maximum value, the rate of dissipation becomes very large, effectively inhibiting any further crystallization. Also, this form satisfies the required conditions as in Eq. (1.63) . For the chosen form of rate of dissipation for phase-2, the rate of crystallization for phase-2 takes the following form:

$$\dot{\alpha}_2 = G_2(\alpha_{2_0} - \alpha_2)^{k_2/m_2 - 1}\left(\left(\frac{\theta_{r_2} - \theta}{\theta_{r_2}}\right) - \frac{1}{\Delta H_a}\frac{\partial i_\psi}{\partial \alpha_2} + \frac{\mu_a(I_{B_{\kappa_a}} - 3)}{2\rho\Delta H_a}\right)^{1/m_2 - 1}, \tag{1.71}$$

Where G_2 is a constant. This completes the formulation for the mixture during second phase change process that takes place at lower temperature.

2.1.5. The semi-crystalline phase after the second crystallization process

At the end of the second crystallization process, the material consists of a mixture of fixed amounts of the amorphous phase, crystalline phase-1 and crystalline phase-2. Behavior of the TSMP is like an anisotropic elastic material. The material has multiple natural configurations associated with it, one for the amorphous phase and a multiplicity of natural configurations for the crystalline phase-1 and crystalline phase-2. Again, note that if the crystallization occurs at a single configuration the crystalline phase will have only one natural configuration. Proceeding in a manner similar to the earlier case, the Helmholtz potential for the material can be given by

$$\psi = i_\psi + (1-\alpha_1-\alpha_2)\psi_a + \int_{t_{s_1}}^{t_{f_2}} \psi_{c_1}\frac{d\alpha_1}{d\tau} d\tau + \int_{t_{s_2}}^{t_{f_2}} \psi_{c_2}\frac{d\alpha_2}{d\tau} d\tau. \tag{1.72}$$

Note that Eq. (1.72) is very similar to Eq. (1.47), other than the change in the limits of integration. This is due to the fact that crystallization of both the crystalline phases stops at time t_{f_2} and the amorphous phase, crystalline phase-1 and crystalline phase-2 are fixed. Hence, the Cauchy stress in the material will also have a form similar to Eq. (1.52) with τ replaced by t_{f_2} in the limits of integration. For the specific forms chosen for the internal energy and entropy for the two crystalline phases the Cauchy stress is similar to Eq. (1.67) with a change in the limits and is given by

$$\begin{aligned} T &= -pI + (1-\alpha_1-\alpha_2)\mu_a B_{\kappa_a} + \int_{t_{s_1}}^{t_{f_2}} \mu_{c_1 1} B_{\kappa_{c_1(\tau)}} \frac{d\alpha_1}{d\tau} d\tau + \int_{t_{s_1}}^{t_{f_2}} (F_{\kappa_{c_1(\tau)}} (\mu_{c_1 1}(J_1-1) n_{\kappa_{c_1(\tau)}} \otimes n_{\kappa_{c_1(\tau)}} \\ &+ \mu_{c_1 2}(K_1-1) m_{\kappa_{c_1(\tau)}} \otimes m_{\kappa_{c_1(\tau)}}) F^{\mathrm{T}}{}_{\kappa_{c_1(\tau)}}) \frac{d\alpha_1}{d\tau} d\tau \\ &+ \int_{t_{s_2}}^{t_{f_2}} \mu_{c_2 1} B_{\kappa_{c_2(\tau)}} \frac{d\alpha_2}{d\tau} d\tau + \int_{t_{s_2}}^{t_{f_2}} (F_{\kappa_{c_2(\tau)}} (\mu_{c_2 1}(J_3-1) n_{\kappa_{c_2(\tau)}} \otimes n_{\kappa_{c_2(\tau)}} \\ &+ \mu_{c_2 2}(K_3-1) m_{\kappa_{c_2(\tau)}} \otimes m_{\kappa_{c_2(\tau)}}) F^{\mathrm{T}}{}_{\kappa_{c_2(\tau)}}) \frac{d\alpha_2}{d\tau} d\tau. \end{aligned} \tag{1.73}$$

2.1.6. Transition of crystalline phase-2 to amorphous phase

On heating to a temperature above the second recovery temperature (t_{r_2}) crystals of phase-2 start to transition to the amorphous phase. The crystalline phase-2 converts to the amorphous phase due to the transition of these crystals and the material becomes more rubber-like. Crystallites of phase-1 and phase-2 that are formed at the lower temperature are responsible for keeping the TSMP in the second temporary shape. As the crystallites of phase-2 melt and disappear the TSMP reverts towards the first temporary shape. When this transformation is complete the material is completely free from crystalline phase-2. The part of phase-1 that crystallizes at lower temperature also contributes to the fixation of second temporary shape, but it melts at a higher temperature and is still present in the material at this point. As a result, the TSMP does not revert back to the first temporary shape completely upon melting of crystallites of phase-2. It is essential to track which fraction of the crystalline phase-2 is undergoing transition at any given time, in order to track the evolution of the shape as it evolves from the second temporary shape towards the first temporary shape. This is particularly true for the case where crystallization takes place while the material is kept loaded, as different crystals are formed at different stretches and can have different stress free states (for details see Barot et al., 2008 and Rao & Rajagopal, 2002). For the constant stretch case, the manner in which the crystals melt does not impact the intermediate shapes occupied by the polymer as all the crystals were formed in the same configuration. However, the manner in which the crystallites melt is important for crystallization under constant stress or for a more general case wherein crystallization takes place under conditions of changing stress and strain. The assumption made with respect to the transition process is that the crystallites formed last melt first. This assumption is supported by experiments as long as crystallites formed last are formed farthest from the equilibrium transition temperature. This is because these crystallites are thinner and melt at a lower temperatures on reheating (see Gedde, 1999, Rao & Rajagopal, 2002 and Rao & Rajagopal, 2000).The Helmholtz potential of the mixture during the transition of phase-2 at any given point of time can be then calculated using the following equation:

$$\psi = i_\psi + (1-\alpha_1-\alpha_2)\psi_a + \int_{t_{s_1}}^{t_{f_2}} \psi_{c_1} \frac{d\alpha_1}{d\tau} d\tau + \int_{t_{s_2}}^{\tau^{**}} \psi_{c_2} \frac{d\alpha_2}{d\tau} d\tau, \tag{1.74}$$

with $\tau^{**} \in [t_{s_2}, t_{f_2}]$ and $\alpha_2(\tau^{**}) = \alpha_2(t)$.

Note that in the above equation the time has been tagged when the material has a prescribed crystallinity of phase-2 during transition to the actual times when the material had the same crystallinity of phase-2 during the crystallization i.e. $\tau^{**} \in [t_{s_2}, t_{f_2}]$. Using the rate equation for transition of phase-2, its current value can be known, and thus, the amount that has melted is also known. Since the crystallinity is tracked as a function of time during crystallization of phase-2, through interpolation between known values of crystallinity and the times at which those values occur; we can determine the time during the crystallization process, denoted by $\tau^{**} \in [t_{s_2}, t_{f_2}]$, when the amount of crystalline material of phase-2 present equals its current level, i.e., $\alpha_2(\tau^{**}) = \alpha_2(t)$. This is possible because of the assumption that crystallites formed later are the first to melt. With this information it is now possible to write the reduced energy dissipation for the transition process with the aid of Eqs. (1.10), (1.74), (1.50) and (1.20) as follows

$$\begin{aligned} &\left(T - (1-\alpha_1-\alpha_2)2\rho\left[F_{\kappa_a} \frac{\partial \psi_a}{\partial C_{\kappa_a}} F^{\mathrm{T}}{}_{\kappa_a}\right] - 2\rho\left[\int_{t_{s_1}}^{t_f} F_{\kappa_{c_1(\tau)}} \frac{\partial \psi_{c_1}}{\partial C_{\kappa_{c_1(\tau)}}} F_{\kappa_{c_1(\tau)}} \frac{d\alpha_1}{d\tau} d\tau\right]\right. \\ &\left. -2\rho\left[\int_{t_{s_2}}^{t_f} F_{\kappa_{c_2(\tau)}} \frac{\partial \psi_{c_2}}{\partial C_{\kappa_{c_2(\tau)}}} F_{\kappa_{c_2(\tau)}} \frac{d\alpha_2}{d\tau} d\tau\right]\right) \cdot D - \rho\left(\frac{\partial \psi}{\partial \theta} + \eta\right)\dot{\theta} \\ &-\rho\left(\psi_{c_2}\Big|_{C_{\kappa_{c_2(\tau)}}=I} - \psi_a\Big|_{C_{\kappa_a}} - \frac{\partial i_\psi}{\partial \alpha_2}\right)\dot{\alpha}_2 = \zeta_m = \zeta_{m_2} \geq 0. \end{aligned} \tag{1.75}$$

with $\tau^{**} \in [t_{s_2}, t_{f_2}]$ and $\alpha_2(\tau^{**}) = \alpha_2(t)$. For Eq. (1.75) to hold the sufficient conditions are that Eq. (1.53) be satisfied and the Cauchy stress satisfy the following:

$$\begin{aligned} T &= -pI + 2(1-\alpha_1-\alpha_2)\rho\left[\frac{\partial \psi_a}{\partial I_B} B_{\kappa_a} + 2\frac{\partial \psi_a}{\partial II_B} B^2{}_{\kappa_a}\right] \\ &+2\rho\left[\int_{t_{s_1}}^{t_{f_2}} F_{\kappa_{c_1(\tau)}} \frac{\partial \psi_{c_1}}{\partial C_{\kappa_{c_1(\tau)}}} F_{\kappa_{c_1(\tau)}} \frac{d\alpha_1}{d\tau} d\tau\right] + 2\rho\left[\int_{t_{s_2}}^{\tau^{**}} F_{\kappa_{c_2(\tau)}} \frac{\partial \psi_{c_2}}{\partial C_{\kappa_{c_2(\tau)}}} F_{\kappa_{c_2(\tau)}} \frac{d\alpha_2}{d\tau} d\tau\right]\Bigg) \end{aligned} \tag{1.76}$$

with $\tau^{**} \in [t_{s_2}, t_{f_2}]$ and $\alpha_2(\tau^{**}) = \alpha_2(t)$. By virtue of this, the reduced energy dissipation equation reduces to:

$$-\rho\left(\psi_{c_2}\Big|_{C_{\kappa_{c_2(\tau)}}=I} - \psi_a\Big|_{C_{\kappa_a}} - \frac{\partial i_\psi}{\partial \alpha_2}\right)\dot{\alpha}_2 = \zeta_m = \zeta_{m_2} \geq 0. \tag{1.77}$$

Note that in the above equation, since the crystalline phase-2 is undergoing transition to the amorphous phase, $\dot{\alpha}_2 \leq 0$. Hence, for crystallization of phase-2 to take place and satisfy the restriction that the rate of dissipation due to transition to the amorphous phase be non-negative $\zeta_{m_2} \geq 0$, the term in the bracket has to be greater than zero. This term acts as the driving force for transition to the amorphous phase:

$$D_{f_2} = \left(\psi_{c_2}\Big|_{C_{K_{c_2(\tau)}}=I} - \psi_a\Big|_{C_{K_a}} - \frac{\partial i_\psi}{\partial \alpha_2} \right). \tag{1.78}$$

We assume that the rate of dissipation due to transition depends on the same parameters as during crystallization of phase-2. However, it is important to note that their specific forms can be different. The rate of dissipation associated with change in phase-2 during transition is given by:

$$\zeta_{m_2} = \zeta_{m_2}(\alpha_2, \dot{\alpha}_2, \theta, ...) \geq 0. \tag{1.79}$$

Moreover, it is reasonable to assume that if transition rate is zero then the rate of dissipation associated with the change in phase-2 during transition to the amorphous phase is also exactly equal to zero:

$$\zeta_{m_2}\Big|_{\dot{\alpha}_2=0} = 0. \tag{1.80}$$

The activation function will depend on the deformation variables associated with the amorphous and both the crystalline phases through their respective Helmholtz potentials. This is because at the instant transition of phase-2 to the amorphous phase is initiated; amorphous phase and both the crystalline phases can be in a deformed state. In such a case the activation function is defined through the driving force as

$$\phi_{m_2}(\theta, B_{K_a}, B_{K_{c_2(\tau^{**})}}) = D_{f_2}\Big|_{\alpha_2=\alpha_{2_0}} - B_2, \tag{1.81}$$

where, B_2 is the initiation barrier and is a positive constant.

When there is no transition the activation function will take negative values and it will be exactly zero when activation is about to begin. Transition of phase-2 to the amorphous phase starts to take place, once the activation function exceeds zero. The activation criterion for the initiation of transition of phase-2 to the amorphous phase can be stated more precisely as follows:

$$\phi_{m_2}(\theta, B_{K_a}, B_{K_{c_2(\tau^{**})}}) > 0 \tag{1.82a}$$

Or

$$\phi_{m_2}(\theta, B_{K_a}, B_{K_{c_2(\tau^{**})}}) = 0\,, \quad \text{and} \quad \frac{\partial \phi_{m_2}}{\partial \theta}\dot{\theta} + \frac{\partial \phi_{m_2}}{\partial B_{K_a}}\dot{B}_{K_a} + \frac{\partial \phi_{m_2}}{\partial B_{K_{c_2(\tau^{**})}}}\dot{B}_{K_{c_2(\tau^{**})}} > 0 \tag{1.82b}$$

This concludes the specification of the initiation criterion for the transition process of crystalline phase-2. Depending on the forms chosen for the various thermodynamic quantities for the amorphous phase and crystalline phase-2 in this work, the activation function for the transition process of phase-2 to the amorphous phase can be written as:

$$\begin{aligned}\phi_2(\theta, B_{K_a}, B_{K_{c_2(\tau^{**})}}) = {} & \left(\frac{\theta-\theta_{r_2}}{\theta_{r_2}}\right) - \frac{1}{\Delta H_a}\frac{\partial i_\psi}{\partial \alpha_2}\Big|_{\alpha_2=\alpha_2(t^{**})} \\ & + \frac{\mu_{c_2}(I_{B_{K_{c_2(\tau^{**})}}} - 3) + \mu_{c_2 1}(J_3-1)^2 + \mu_{c_2 2}(K_3-1)^2 - \mu_a(I_{B_{K_a}}-3)}{2\rho\Delta H_a}.\end{aligned} \tag{1.83}$$

It is important to prescribe the rate of dissipation associated with the phase change during the transition process, for derivation of the rate of transition of crystalline phase-2 to the amorphous phase. In this work we choose the simplest form that depends on the crystallinity of phase-2 and the crystallization rate associated with it, namely

$$\zeta_{m_2} = \frac{|\dot{\alpha}_2|^{m_2}}{\bar{G}(\dot{\alpha}_2)^{k_2}}. \tag{1.84}$$

It is important to note that the chosen form for ζ_{m_2} is very similar to the rate of dissipation associated with the phase transition of phase-2 during crystallization i.e. ζ_{p_2}. For the chosen form forζ_{m_2}, the transition rate can be prescribed using Eqs. (1.77) and (1.83) as follows:

$$\begin{aligned}\dot{\alpha}_2 = {} & -G_2(\alpha_2)^{k_2/m_2-1}\left(\left(\frac{\theta-\theta_{r_2}}{\theta_{r_2}}\right) - \frac{1}{\Delta H_a}\frac{\partial i_\psi}{\partial \alpha_2}\right. \\ & \left. + \frac{\mu_{c_2}(I_{B_{K_{c_2(\tau^{**})}}} - 3) + \mu_{c_2 1}(J_3-1)^2 + \mu_{c_2 2}(K_3-1)^2 - \mu_a(I_{B_{K_a}}-3)}{2\rho\Delta H_a}\right)^{1/m_2-1}.\end{aligned} \tag{1.85}$$

For the specific choices made for the stored energy functions for the amorphous phase and both the crystalline phases the Cauchy stress is given by:

$$T = -pI + (1-\alpha_1-\alpha_2)\mu_a B_{\kappa_a} + \int_{t_{s_1}}^{t_{f_2}} \mu_{c_11} B_{\kappa_{c_1(\tau)}} \frac{d\alpha_1}{d\tau_1} d\tau_1 + \int_{t_{s_2}}^{\tau^{**}} \mu_{c_21} B_{\kappa_{c_2(\tau)}} \frac{d\alpha_2}{d\tau} d\tau$$
$$+ \int_{t_{s_1}}^{t_{f_2}} (F_{\kappa_{c_1(\tau)}} (\mu_{c_11}(J_1-1) n_{\kappa_{c_1(\tau)}} \otimes n_{\kappa_{c_1(\tau)}} + \mu_{c_12}(K_1-1) m_{\kappa_{c_1(\tau)}} \otimes m_{\kappa_{c_1(\tau)}}) F^{T}_{\kappa_{c_1(\tau)}}) \frac{d\alpha_1}{d\tau_1} d\tau_1 \tag{1.86}$$
$$+ \int_{t_{s_2}}^{\tau^{**}} (F_{\kappa_{c_2(\tau)}} (\mu_{c_21}(J_3-1) n_{\kappa_{c_2(\tau)}} \otimes n_{\kappa_{c_2(\tau)}} + \mu_{c_22}(K_3-1) m_{\kappa_{c_2(\tau)}} \otimes m_{\kappa_{c_2(\tau)}}) F^{T}_{\kappa_{c_2(\tau)}}) \frac{d\alpha_2}{d\tau} d\tau$$

with $\tau^{**} \in [t_{s_2}, t_{f_2}]$ and $\alpha_2(\tau^{**}) = \alpha_2(t)$.

With the internal energy of the second phase, the specific form of the energy equation for the mixture under consideration is derived. Moreover, there is no stress in the material during heating, the material is totally unloaded. For this situation the energy equation can be assumed to take the form:

$$\rho((1-\alpha_1-\alpha_2)C_a + \alpha_1 C_{c_1} + \alpha_2 C_{c_2})\dot{\theta} + \mathrm{div}\mathbf{q}$$
$$= (1-\alpha_1-\alpha_2)\mu_a B_{\kappa_a} \cdot L + \rho\left(C_a\theta + A_a - C_{c_2}\theta - A_{c_2} - \frac{\partial i_\psi}{\partial \alpha_2}\right)\dot{\alpha}_2 + \rho r \tag{1.87}$$

2.1.7. Melting of the first crystalline phase

On heating above the first recovery temperature θ_{r_1} the material reverts to the original shape. Once the temperature goes above the first recovery temperature, the crystals of phase-1 (formed both at the lower and higher temperatures) start to transition to the amorphous phase. As this happens the crystallites, which are responsible for keeping the TSMP in the first temporary shape disappear. When this transformation is complete the material returns to the permanent shape and is completely free from the crystalline phase. Proceeding in a manner similar to the previous case, the Helmholtz potential of the mixture during the transition of phase-1 at any given point of time can be then calculated using the following equation:

$$\psi = i_\psi + (1-\alpha_1)\psi_a + \int_{t_{s_1}}^{\tau^*} \psi_{c_1} \frac{d\alpha_1}{d\tau} d\tau \tag{1.88}$$

With $\tau^* \in [t_{s_1}, t_{f_2}]$ and $\alpha_1(\tau^*) = \alpha_1(t)$.

Current value of crystallinity of phase-1 and amount that has melted are calculated using similar methodology as used for phase-2. The reduced energy dissipation, for the transition process with the aid of Eqs. (1.10), (1.20) and (1.88) can be written as follows

$$\left(T - (1-\alpha_1)2\rho\left[F_{\kappa_a} \frac{\partial \psi_a}{\partial C_{\kappa_a}} F^{T}_{\kappa_a}\right] - 2\rho\left[\int_{t_{s_1}}^{\tau^*} F_{\kappa_{c_1(\tau)}} \frac{\partial \psi_{c_1}}{\partial C_{\kappa_{c_1(\tau)}}} F_{\kappa_{c_1(\tau)}} \frac{d\alpha_1}{d\tau} d\tau\right]\right) \cdot D$$
$$-\rho\left(\frac{\partial \psi}{\partial \theta} + \eta\right)\dot{\theta} - \rho\left(\psi_{c_1}\Big|_{C_{\kappa_{c_1(\tau)}}=I} - \psi_a\Big|_{C_{\kappa_a}} - \frac{\partial i_\psi}{\partial \alpha_1}\right)\dot{\alpha}_1 = \xi_m = \xi_{m_1} \geq 0. \tag{1.89}$$

with $\tau^* \in [t_{s_1}, t_{f_2}]$ and $\alpha_1(\tau^*) = \alpha_1(t)$. For Eq. (1.89) to hold the sufficient conditions are that Eq. (1.23) be satisfied and the Cauchy stress satisfy the following

$$T = -pI + 2(1-\alpha_1)\rho\left[\frac{\partial \psi_a}{\partial I_B} B_{\kappa_a} + 2\frac{\partial \psi_a}{\partial II_B} B^2{}_{\kappa_a}\right] + 2\rho\left[\int_{t_{s_1}}^{\tau^*} F_{\kappa_{c_1(\tau)}} \frac{\partial \psi_{c_1}}{\partial C_{\kappa_{c_1(\tau)}}} F_{\kappa_{c_1(\tau)}} \frac{d\alpha_1}{d\tau} d\tau\right] \tag{1.90}$$

with $\tau^* \in [t_{s_1}, t_{f_2}]$ and $\alpha_1(\tau^*) = \alpha_1(t)$. By virtue of this, the reduced energy dissipation equation reduces to:

$$-\rho\left(\psi_{c_1}\Big|_{C_{\kappa_{c_1(\tau)}}=I} - \psi_a\Big|_{C_{\kappa_a}} - \frac{\partial i_\psi}{\partial \alpha_1}\right)\dot{\alpha}_1 = \zeta_m = \zeta_{m_1} \geq 0. \tag{1.91}$$

Since the crystalline phase-1 is undergoing transition to the amorphous phase, $\dot{\alpha}_1 \leq 0$. Hence, for crystallization of phase-1 to take place and satisfy the restriction that the rate of dissipation due to transition to the amorphous phase be non-negative $\zeta_{m_1} \geq 0$, the term in the bracket has to be greater than zero. This term acts as the driving force for transition of phase-1 to the amorphous phase:

$$D_{f_1} = \left(\psi_{c_1}\Big|_{C_{\kappa_{c_1(\tau)}}=I} - \psi_a\Big|_{C_{\kappa_a}} - \frac{\partial i_\psi}{\partial \alpha_1}\right). \tag{1.92}$$

As discussed earlier we assume that the rate of dissipation due to transition depends on the same parameters as during crystallization of phase-1. However, it is important to note that their specific forms can be different. The rate of dissipation associated with the change of phase-1 during transition is given by:

$$\zeta_{m_1} = \zeta_{m_1}(\alpha_1, \dot{\alpha}_1, \theta, \ldots) \geq 0. \tag{1.93}$$

Moreover, it is reasonable to assume that if transition rate is zero, then the rate of dissipation associated with the phase change during transition to the amorphous phase is also exactly equal to zero:

$$\zeta_{m_1}\Big|_{\dot{\alpha}_1=0} = 0. \tag{1.94}$$

At the instant transition to the amorphous phase is initiated, both phases can be in a deformed state. As a result as explained earlier, the activation function will depend on the deformation variables associated with the amorphous phase and

crystalline phase-1 through their respective Helmholtz potentials. In such a case the activation function is defined through the driving force as

$$\phi_{m_1}(\theta, B_{\kappa_a}, B_{\kappa_{c_1(\tau^*)}}) = D_{f_1}\big|_{\alpha_1=\alpha_{1_0}} - B_1, \tag{1.95}$$

where B_1, is the initiation barrier and is a positive constant.

The activation function for phase-1 will take negative values when there is no transition and it will be exactly zero when activation is about to begin. Once the activation function exceeds zero, transition of phase-1 to the amorphous phase takes place. The activation criterion for the initiation of transition to the amorphous phase can be stated more precisely as follows:

$$\phi_{m_1}(\theta, B_{\kappa_a}, B_{\kappa_{c_1(\tau^*)}}) > 0 \tag{1.96a}$$

Or

$$\phi_{m_1}(\theta, B_{\kappa_a}, B_{\kappa_{c_1(\tau^*)}}) = 0\,, \quad \text{and} \quad \frac{\partial \phi_{m_1}}{\partial \theta}\dot{\theta} + \frac{\partial \phi_{m_1}}{\partial B_{\kappa_a}}\dot{B}_{\kappa_a} + \frac{\partial \phi_{m_1}}{\partial B_{\kappa_{c_1(\tau^*)}}}\dot{B}_{\kappa_{c_1(\tau^*)}} > 0. \tag{1.96b}$$

This completes the specification of the initiation criterion for the transition process of crystalline phase-1. Depending on the chosen forms for the various thermodynamic quantities for the amorphous phase and crystalline phase-1 in this work, the activation function for the transition process of phase-1 to the amorphous phase can be written as:

$$\begin{aligned}\phi_1(\theta, B_{\kappa_a}, B_{\kappa_{c_1(\tau^*)}}) = {} & \left(\frac{\theta-\theta_{r_1}}{\theta_{r_1}}\right) - \frac{1}{\Delta H_a}\frac{\partial i_\psi}{\partial \alpha_1}\Big|_{\alpha_1=\alpha_1(t^*)} \\ & + \frac{\mu_{c_1}(I_{B_{\kappa_{c_1(\tau^*)}}}-3)+\mu_{c_1 1}(J_1-1)^2+\mu_{c_1 2}(K_1-1)^2-\mu_a(I_{B_{\kappa_a}}-3)}{2\rho\Delta H_a}.\end{aligned} \tag{1.97}$$

Prescription of the rate of dissipation associated with the phase change during the transition process is required for deriving the rate of transition of crystalline phase-1 to amorphous phase. In this work we choose the simplest form that depends on the crystallinity and the crystallization rate of phase-1, namely

$$\zeta_{m_1} = \frac{|\dot{\alpha}_1|^{m_1}}{\bar{G}(\dot{\alpha}_1)^{k_1}}. \tag{1.98}$$

It is important to note that the chosen form for ζ_{m_1} is very similar to the rate of dissipation associated with the phase transition of phase-1 during crystallization i.e. ζ_{p_1}. For the chosen form forζ_{m_1}, the transition rate can be prescribed using Eqs. (1.91) and (1.97) as follows:

$$\begin{aligned}\dot{\alpha}_1 = {} & -G_1(\alpha_1)^{k_1/m_1-1}\Bigg(\left(\frac{\theta-\theta_{r_1}}{\theta_{r_1}}\right) - \frac{1}{\Delta H_a}\frac{\partial i_\psi}{\partial \alpha_1} \\ & + \frac{\mu_{c_1}(I_{B_{\kappa_{c_1(\tau^*)}}}-3)+\mu_{c_1 1}(J_1-1)^2+\mu_{c_1 2}(K_1-1)^2-\mu_a(I_{B_{\kappa_a}}-3)}{2\rho\Delta H_a}\Bigg)^{1/m_1-1}.\end{aligned} \tag{1.99}$$

For the specific choices made for the stored energy functions for the amorphous and crystalline phase-1 the Cauchy stress is given by:

$$\begin{aligned}T = {} & -pI + (1-\alpha_1)\mu_a B_{\kappa_a} + \int_{t_{s_1}}^{\tau^*}\mu_{c_1 1}B_{\kappa_{c_1(\tau_1)}}\frac{d\alpha_1}{d\tau_1}d\tau_1 + \int_{t_{s_1}}^{\tau^*}(F_{\kappa_{c_1(\tau)}}(\mu_{c_1 1}(J_1-1)n_{\kappa_{c_1(\tau)}}\otimes n_{\kappa_{c_1(\tau)}} \\ & +\mu_{c_1 2}(K_1-1)m_{\kappa_{c_1(\tau)}}\otimes m_{\kappa_{c_1(\tau)}})F^{\mathrm{T}}{}_{\kappa_{c_1(\tau)}})\frac{d\alpha_1}{d\tau}d\tau\end{aligned} \tag{1.100}$$

with $\tau^* \in [t_{s_1}, t_{f_2}]$ and $\alpha_1(\tau^*) = \alpha_1(t)$. As the material is unloaded during heating, there is no stress in the material, and the energy equation can be assumed to take the form:

$$\begin{aligned}\rho((1-\alpha_1)C_a + \alpha_1 C_{c_1})\dot{\theta} + \mathrm{div}q = {} & (1-\alpha_1)\mu_a B_{\kappa_a}\cdot L \\ & + \rho\left(C_a\theta + A_a - C_{c_1}\theta - A_{c_1} - \frac{\partial i_\psi}{\partial \alpha_1}\right)\dot{\alpha}_1 + \rho r.\end{aligned} \tag{1.101}$$

This concludes the formulation of the constitutive equations. In the next section a specific boundary value problem is solved using the governing equations.

Section 3: Application of the constitutive model

3.1. Application of the model to inflation and extension of a hollow cylinder

Inflation and extension of a hollow cylinder made with TSMP is examined here and set of equations governing the thermo-mechanical cycle associated with it are presented. These equations are then solved for a complete cycle. Inflation and extension of the hollow cylinder is an inhomogeneous deformation and for this case it is assumed that the rates at which the cylinder is inflated and extended are slow and hence, inertial terms have been ignored. Here, in this problem, we keep the stretch ratio ($\Lambda(t)$) constant in all the processes: loading-1, cooling-1, unloading-1, loading-2, cooling-2, unloading-2, heating-1 and heating-2.

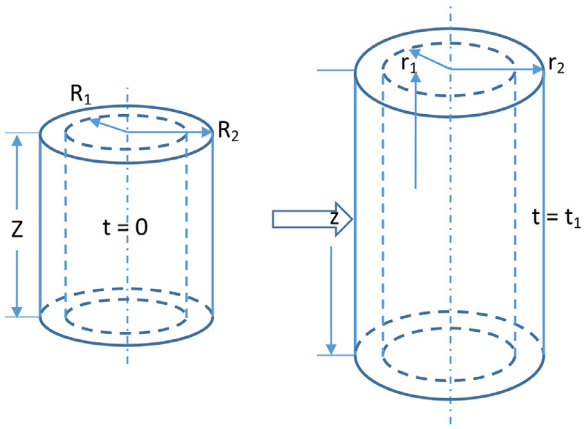

Fig. 5. Schematic illustration associated with the inflation and extension of a hollow cylinder.

3.1.1. Kinematics

Consider the Fig. 5 showing a hollow cylinder with internal radius R_1, external radius R_2 and height H at time $t = 0$. We use cylindrical co-ordinates (R, Θ, Z) for the purpose of analysis. The material is stretched in z-direction and the tube is pressurized gradually to inflate the tube in such a way that motion is given by:

$$r = r(R,t),\ \vartheta = \Theta,\ z = \Lambda Z. \tag{2.1}$$

For the given case, the deformation gradients F_{κ_a} and $F_{\kappa_{c(\tau)}}$ can be written as:

$$F_{\kappa_a} = \begin{pmatrix} \frac{dr(R,t)}{dR} & 0 & 0 \\ 0 & \frac{r(R,t)d\Theta}{Rd\Theta} & 0 \\ 0 & 0 & \Lambda(t) \end{pmatrix}, F_{\kappa_{c_1(\tau)}} = \begin{pmatrix} \frac{dr(R,t)}{dr(R,\tau)} & 0 & 0 \\ 0 & \frac{r(R,t)}{r(R,\tau)} & 0 \\ 0 & 0 & \frac{\Lambda(t)}{\Lambda(\tau)} \end{pmatrix}, F_{\kappa_{c_2(\tau)}} = \begin{pmatrix} \frac{dr(R,t)}{dr(R,\tau)} & 0 & 0 \\ 0 & \frac{r(R,t)}{r(R,\tau)} & 0 \\ 0 & 0 & \frac{\Lambda(t)}{\Lambda(\tau)} \end{pmatrix}. \tag{2.2}$$

The equation for the conservation of mass reduces to the constraint of incompressibility:

$$\det(F) = 1. \tag{2.3}$$

According to the conservation of mass given by Eq. (2.3) and based on the assumption that stretch ratio remains constant throughout the deformation cycle, the deformation gradients take the following forms:

$$F_{\kappa_a} = \begin{pmatrix} \frac{R}{\Lambda r(R,t)} & 0 & 0 \\ 0 & \frac{r(R,t)}{R} & 0 \\ 0 & 0 & \Lambda \end{pmatrix}, F_{\kappa_{c_1(\tau)}} = \begin{pmatrix} \frac{r(\tau)}{r(t)} & 0 & 0 \\ 0 & \frac{r(t)}{r(\tau)} & 0 \\ 0 & 0 & 1 \end{pmatrix}, F_{\kappa_{c_2(\tau)}} = \begin{pmatrix} \frac{r(\tau)}{r(t)} & 0 & 0 \\ 0 & \frac{r(t)}{r(\tau)} & 0 \\ 0 & 0 & 1 \end{pmatrix}. \tag{2.4}$$

The other important kinematic tensors such as B_{κ_a}, C_{κ_a}, $B_{\kappa_{c_1(\tau)}}$, $C_{\kappa_{c_1(\tau)}}$, $B_{\kappa_{c_2(\tau)}}$, $C_{\kappa_{c_2(\tau)}}$ can be expressed as

$$B_{\kappa_a} = C_{\kappa_a} = \begin{pmatrix} \left(\frac{R}{\Lambda r(R,t)}\right)^2 & 0 & 0 \\ 0 & \left(\frac{r(R,t)}{R}\right)^2 & 0 \\ 0 & 0 & (\Lambda)^2 \end{pmatrix}, \tag{2.5}$$

$$B_{\kappa_{c_1(\tau)}} = C_{\kappa_{c_1(\tau)}} = \begin{pmatrix} \left(\frac{r(\tau)}{r(t)}\right)^2 & 0 & 0 \\ 0 & \left(\frac{r(t)}{r(\tau)}\right)^2 & 0 \\ 0 & 0 & 1 \end{pmatrix}, \quad B_{\kappa_{c_2(\tau)}} = C_{\kappa_{c_2(\tau)}} = \begin{pmatrix} \left(\frac{r(\tau)}{r(t)}\right)^2 & 0 & 0 \\ 0 & \left(\frac{r(t)}{r(\tau)}\right)^2 & 0 \\ 0 & 0 & 1 \end{pmatrix}, \tag{2.6}$$

The directions of the orthotropy in the crystalline phase formed at time τ is determined by the unit vectors $n_{\kappa_{c_1(\tau)}}$, $m_{\kappa_{c_1(\tau)}}$,$n_{\kappa_{c_2(\tau)}}$ and $m_{\kappa_{c_2(\tau)}}$, which in turn are the eigenvectors of B_{κ_a} at the time of formation of the crystalline phase. We can define $n_{\kappa_{c_1(\tau)}}$, $m_{\kappa_{c_1(\tau)}}$,$n_{\kappa_{c_2(\tau)}}$ and $m_{\kappa_{c_2(\tau)}}$ through:

$$n_{\kappa_{c_1(\tau)}} = \begin{pmatrix} 1 \\ 0 \\ 0 \end{pmatrix}, \quad m_{\kappa_{c_1(\tau)}} = \begin{pmatrix} 0 \\ 1 \\ 0 \end{pmatrix}, n_{\kappa_{c_2(\tau)}} = \begin{pmatrix} 1 \\ 0 \\ 0 \end{pmatrix}, \quad m_{\kappa_{c_2(\tau)}} = \begin{pmatrix} 0 \\ 1 \\ 0 \end{pmatrix}. \tag{2.7}$$

These eigenvectors are required to find the invariants associated with anisotropy such as J_1, K_1, J_2 and K_2.

3.1.2. Mass conservation

For the current problem, the balance of mass is given by the Eq. (2.3) but a more useful form of the balance law can be written using Eqs. (2.2) and (2.3) applying proper limits. We obtain that

$$r^2 - r^2{}_1 = \frac{1}{\Lambda}(R^2 - R^2{}_1). \tag{2.8}$$

This is a useful equation because knowing R_1 and r_1 the distance of each particle from the reference configuration to the deformed configuration or to the current configuration can be mapped.

3.1.3. Balance of linear momentum

For the current geometry the balance of linear momentum in cylindrical co-ordinates can be written as follows:

$$\frac{d\sigma_{rr}}{dr} = \frac{1}{r}(\sigma_{\vartheta\vartheta} - \sigma_{rr}). \tag{2.9}$$

But we know that

$$\begin{aligned} \sigma_{rr}(r_1) &= -P_i, \\ \sigma_{rr}(r_2) &= -P_o, \end{aligned} \tag{2.10}$$

where, P_i, is the internal pressure and P_o is ambient pressure that is applied to the outer wall of the cylinder. Using Eq. (2.9) and the boundary conditions given in Eq. (2.10) a relation between pressure difference and radii can be prescribed as given below.

$$\Delta P = P_i - P_o = \int_{r_1}^{r_2} \frac{\sigma_{\vartheta\vartheta} - \sigma_{rr}}{r} dr. \tag{2.11}$$

3.1.4. Conservation of energy

Heat conduction is the primary mode of the thermal energy transfer inside the material. It is assumed that at the outer surface of the cylinder, the temperature drops linearly while cooling and increases linearly while heating and the inner surface of the cylinder is insulated. It is also assumed that there is no heat transfer possible from the top and the bottom of the cylinder. Hence, at a particular radius r in all $r-\vartheta$ planes, material points will have the same temperature. Simplifying Eq. (1.68) for the geometry under consideration, the energy equation reduces to a heat conduction equation with source terms for heat due to phase change and entropic changes in the polymer. This equation is given by:

$$\frac{\partial\theta}{\partial t} = \gamma\left(\frac{\partial^2\theta}{\partial r^2} + \frac{1}{r}\frac{\partial\theta}{\partial r}\right) + \frac{\Delta H_a}{C_a}\dot{\alpha}_1 + \frac{\Delta H_a}{C_a}\dot{\alpha}_2 + \frac{\mu_a(1-\alpha_1-\alpha_2)B_{\kappa_a}\cdot L}{c}, \tag{2.12}$$

With the following initial and boundary conditions

$$\theta(r,0) = \theta_{initial}, \quad \frac{\partial\theta(r_1,t)}{\partial r} = 0, \quad \frac{\partial\theta(r_2,t)}{\partial t} = -K, \tag{2.13}$$

Whereγ, ΔH_a, and C_a are the diffusivity, the latent heat and the specific heat of the material respectively and K has a constant positive value during cooling and a constant negative value while heating (thus K cannot be viewed as a constant).

3.2. Method of solution

For the kinematics assumed the balance laws for stress, temperature, crystallization rates for phase-1 and phase-2 etc., are solved. The details for each step of the triple shape cycle are described below.

3.2.1. Loading-1

During the loading-1 process the material is at a temperature θ_H above both the transition temperatures ($\theta_L < \theta_{r_2} < \theta_M < \theta_{r_1} < \theta_H$). Above the transition temperatures there will be no crystallization and hence, crystallinity is identically zero and the polymer is in its amorphous phase. For the amorphous region, the Cauchy stress tensor components can be defined using Eqs. (1.11) and (2.5) as follows:

$$\sigma_{\vartheta\vartheta} = -p + \mu_a\left(\frac{r}{R}\right)^2, \ \sigma_{rr} = -p + \mu_a\left(\frac{R}{\Lambda r}\right)^2, \ \sigma_{zz} = -p + \mu_a(\Lambda)^2. \tag{2.14}$$

Now using Eq. (2.11) the relation between the pressure difference and radii can be established as

$$\Delta P = \mu_a \int_{r_1}^{r_2} \frac{\left(\frac{r}{R}\right)^2 - \left(\frac{R}{\Lambda r}\right)^2}{r} dr. \tag{2.15}$$

3.2.2. Cooling-1

The object is cooled in a specific fashion during this cycle. At the outer radius, the temperature drops linearly whereas at the inner radius the cylinder is insulated. The cooling rate is given by Eq. (2.12), with the boundary conditions given by Eq. (2.13). In this problem during crystallization since the material is not deforming, the velocity is identically equal to zero. In such a scenario, the cooling rate will be given by

$$\frac{\partial\theta}{\partial t} = \gamma\left(\frac{\partial^2\theta}{\partial r^2} + \frac{1}{r}\frac{\partial\theta}{\partial r}\right) + \frac{\Delta H_a}{C_a}\dot{\alpha}_1. \tag{2.16}$$

The required crystallization rate for phase-1 can be prescribed by Eq. (1.39), with the above boundary conditions. Here we note that there is insufficient experimental information available to choose appropriate forms for the interfacial components and the impact of stretching on the crystallization rate. In this work we ignore them with the tacit assumption that appropriate forms can be easily included in the model present here. With these considerations, the equation governing the crystallization will take form:

$$\dot{\alpha}_1 = G_1(\alpha_{0_1} - \alpha_1)^{k_1/m_1 - 1}\left(\frac{\theta_{r_1} - \theta}{\theta_{r_1}}\right)^{1/m_1 - 1} \tag{2.17}$$

Using the constitutive equations developed earlier for the phase transition (amorphous phase to semi-crystalline phase), Eqs. (2.5) and (2.6), and the appropriate forms for the other required scalars such as J_1 and K_1 for phase-1, we can write down the two useful non-zero components of the stress tensor for this process as follows:

$$\begin{aligned}
\sigma_{\vartheta\vartheta} &= -p + (1-\alpha_1(t))\mu_a\left(\frac{r}{R}\right)^2 + \mu_{c_1 1}\int_{t_{s_1}}^{t}\left(\frac{r(t)}{r(\tau)}\right)^2\frac{d\alpha_1}{d\tau}d\tau + \mu_{c_1 2}\int_{t_{s_1}}^{t}\left(\left(\frac{r(t)}{r(\tau)}\right)^4 - \left(\frac{r(t)}{r(\tau)}\right)^2\right)\frac{d\alpha_1}{d\tau}d\tau,\\
\sigma_{rr} &= -p + (1-\alpha_1(t))\mu_a\left(\frac{R}{\Lambda r}\right)^2 + \mu_{c_1 1}\int_{t_{s_1}}^{t}\left(\frac{r(\tau)}{r(t)}\right)^2\frac{d\alpha_1}{d\tau}d\tau + \mu_{c_1 2}\int_{t_{s_1}}^{t}\left(\left(\frac{r(\tau)}{r(t)}\right)^4 - \left(\frac{r(\tau)}{r(t)}\right)^2\right)\frac{d\alpha_1}{d\tau}d\tau.
\end{aligned} \tag{2.18}$$

Using Eq. (2.18) the balance of linear momentum, Eq. (2.11) for the cooling-1 process is given by

$$\Delta P = \int_{r_1}^{r_2}\times\left(\frac{(1-\alpha_1(t))\mu_a\left(\left(\frac{r}{R}\right)^2 - \left(\frac{1}{\Lambda}\frac{R}{r}\right)^2\right) + \mu_{c_1 1}\int_{t_{s_1}}^{t}\left(\left(\frac{r(t)}{r(\tau)}\right)^2 - \left(\frac{r(\tau)}{r(t)}\right)^2\right)\frac{d\alpha_1}{d\tau}d\tau}{r} + \frac{\int_{t_{s_1}}^{t}\left[\mu_{c_1 2}\left(\left(\frac{r(t)}{r(\tau)}\right)^4 - \left(\frac{r(t)}{r(\tau)}\right)^2\right) - \mu_{c_1 1}\left(\left(\frac{r(\tau)}{r(t)}\right)^4 - \left(\frac{r(\tau)}{r(t)}\right)^2\right)\frac{d\alpha_1}{d\tau}d\tau\right]}{r}dr\right) \tag{2.19}$$

3.2.3. Unloading-1

During the unloading-1 process the material is at temperature θ_M which is below the first transition temperature $\theta_{r_1}(\theta_L < \theta_{r_2} < \theta_M < \theta_{r_1} < \theta_H)$ and the crystallization of phase-1 ceases. The crystallinity of phase-1 has reached its maximum value at temperature $\theta = \theta_M$, and cannot increase until temperature has dropped further. Material is unloaded by reducing the internal pressure. Once the pressure inside and outside of the cylinder are equal, the unloading process ends and at the end of the process, the cylinder will go to a configuration between the original configuration (the natural configuration of the amorphous phase) and that of the crystalline phase-1. The equation for the components of the stress tensor will be similar to Eq. (2.18) with the difference in the limits of integrals; the upper limit of the integral in this case would be t_{f_1}.

3.2.4. Loading-2

During the loading-2 process the material is above the transition temperature of phase-2. Above this transition temperature there will be no crystallization of phase-2 and hence, crystallinity is identically zero for phase-2. Loading is achieved by increasing the internal pressure. The material is a mixture of the amorphous phase and crystalline phase-1. The Cauchy stress components and the relationship between pressure differences to radii can be written in a manner similar to unloading-1.

3.2.5. Cooling-2

During the second cooling cycle, the object is cooled in a manner similar to the first cooling process. The cooling rate and the boundary conditions are again given by Eq. (2.12) and Eq. (2.13), respectively. As explained earlier the cooling rate can be given by

$$\frac{\partial\theta}{\partial t} = \gamma\left(\frac{\partial^2\theta}{\partial r^2} + \frac{1}{r}\frac{\partial\theta}{\partial r}\right) + \frac{\Delta H_a}{C_a}\dot{\alpha}_1 + \frac{\Delta H_a}{C_a}\dot{\alpha}_2. \tag{2.20}$$

As the temperature is reduced during the second cooling process phase-1 continues to crystallize. The equation governing the crystallization of phase-1 will take the form similar to Eq. (2.17) given by

$$\dot{\alpha}_1 = G_1(\alpha_{0_1} - \alpha_1)^{k_1/m_1 - 1}\left(\frac{\theta_{r_1} - \theta}{\theta_{r_1}}\right)^{1/m_1 - 1} \tag{2.21}$$

Here α_{0_1} will have a higher value as compared to Cooling-1. With the above boundary conditions, the required crystallization rate for phase-2 can be prescribed by Eq. (1.71). As explained earlier, the equation governing the crystallization rate for phase-2 will take form:

$$\dot{\alpha}_2 = G_2(\alpha_{0_2} - \alpha_2)^{k_2/m_2-1}\left(\frac{\theta_{r_2} - \theta}{\theta_{r_2}}\right)^{1/m_2-1} \tag{2.22}$$

Using the constitutive equations developed for the phase transition, Eqs. (2.5) and (2.6), the appropriate forms for the other required scalars such as J_1, K_1, J_3 and K_3, the two non-zero components of the stress tensor are as follows:

$$\begin{aligned}
\sigma_{\vartheta\vartheta} &= -p + (1-\alpha_1(t)-\alpha_2(t))\mu_a\left(\tfrac{r}{R}\right)^2 + \mu_{c_1 1}\int_{t_{s_1}}^{t}\left(\tfrac{r(t)}{r(\tau)}\right)^2\tfrac{d\alpha_1}{d\tau}d\tau + \mu_{c_1 2}\int_{t_{s_1}}^{t}\left(\left(\tfrac{r(t)}{r(\tau)}\right)^4 - \left(\tfrac{r(t)}{r(\tau)}\right)^2\right)\tfrac{d\alpha_1}{d\tau}d\tau \\
&\quad + \mu_{c_2 1}\int_{t_{s_2}}^{t}\left(\tfrac{r(t)}{r(\tau)}\right)^2\tfrac{d\alpha_2}{d\tau}d\tau + \mu_{c_2 2}\int_{t_{s_2}}^{t}\left(\left(\tfrac{r(t)}{r(\tau)}\right)^4 - \left(\tfrac{r(t)}{r(\tau)}\right)^2\right)\tfrac{d\alpha_2}{d\tau}d\tau \\
\sigma_{rr} &= -p + (1-\alpha_1(t)-\alpha_2(t))\mu_a\left(\tfrac{R}{\Lambda r}\right)^2 + \mu_{c_1 1}\int_{t_{s_1}}^{t}\left(\tfrac{r(\tau)}{r(t)}\right)^2\tfrac{d\alpha_1}{d\tau}d\tau + \mu_{c_1 2}\int_{t_{s_1}}^{t}\left(\left(\tfrac{r(\tau)}{r(t)}\right)^4 - \left(\tfrac{r(\tau)}{r(t)}\right)^2\right)\tfrac{d\alpha_1}{d\tau}d\tau \\
&\quad + \mu_{c_2 1}\int_{t_{s_2}}^{t}\left(\tfrac{r(\tau)}{r(t)}\right)^2\tfrac{d\alpha_2}{d\tau}d\tau + \mu_{c_2 2}\int_{t_{s_2}}^{t}\left(\left(\tfrac{r(\tau)}{r(t)}\right)^4 - \left(\tfrac{r(\tau)}{r(t)}\right)^2\right)\tfrac{d\alpha_2}{d\tau}d\tau
\end{aligned} \tag{2.23}$$

Using Eq. (2.23) the balance of linear momentum, Eq. (2.11) for Cooling-2 process can be given by

$$\Delta P = \int_{r_1}^{r_2}\times\left(\frac{(1-\alpha_1(t)-\alpha_2(t))\mu_a\left(\left(\frac{r}{R}\right)^2-\left(\frac{1}{\Lambda}\frac{R}{r}\right)^2\right)+\mu_{c_1 1}\int_{t_{s_1}}^{t}\left(\left(\frac{r(t)}{r(\tau)}\right)^2-\left(\frac{r(\tau)}{r(t)}\right)^2\right)\frac{d\alpha_1}{d\tau}d\tau}{r}\right.$$
$$\frac{+\int_{t_{s_1}}^{t}\left[\mu_{c_1 2}\left(\left(\frac{r(t)}{r(\tau)}\right)^4-\left(\frac{r(t)}{r(\tau)}\right)^2\right)-\mu_{c_1 1}\left(\left(\frac{r(\tau)}{r(t)}\right)^4-\left(\frac{r(\tau)}{r(t)}\right)^2\right)\frac{d\alpha_1}{d\tau}d\tau\right]}{r}\frac{+\mu_{c_2 1}\int_{t_{s_2}}^{t}\left(\left(\frac{r(t)}{r(\tau)}\right)^2-\left(\frac{r(\tau)}{r(t)}\right)^2\right)\frac{d\alpha_2}{d\tau}d\tau}{r} \tag{2.24}$$
$$\left.\frac{+\int_{t_{s_2}}^{t}\left[\mu_{c_2 2}\left(\left(\frac{r(t)}{r(\tau)}\right)^4-\left(\frac{r(t)}{r(\tau)}\right)^2\right)-\mu_{c_2 1}\left(\left(\frac{r(\tau)}{r(t)}\right)^4-\left(\frac{r(\tau)}{r(t)}\right)^2\right)\frac{d\alpha_2}{d\tau}d\tau\right]}{r}dr\right)$$

3.2.6. Unloading-2

During the second unloading process the material is at temperature θ_L which is below both the transition temperatures ($\theta_L < \theta_{r_2} < \theta_M < \theta_{r_1} < \theta_H$) and the crystallization process ceases. The crystallinity for both the phases having reached its maximum value at time $t = t_{f_2}$, the crystallization ends. Unloading is again achieved in a manner similar to unloading-1. At the end of the process, the cylinder will go to a configuration between the configuration after unloading-1 and the configuration of both the crystalline phases which were formed below θ_M. The equation for the components of the stress tensor will be similar to Eq. (2.23) with the difference that the upper limit of the integral is given by t_{f_2}.

3.2.7. Heating-1

During the heating-1 process, the material is heated above the second transition temperature θ_{r_2}, and the crystallites of phase-2 melt. Heating of the hollow cylinder is similar to the cooling processes, except now the temperature of the outer cylinder increases linearly. The energy equation reduces to:

$$\frac{\partial\theta}{\partial t} = \gamma\left(\frac{\partial^2\theta}{\partial r^2} + \frac{1}{r}\frac{\partial\theta}{\partial r}\right) - \frac{\Delta H_a}{C_a}\dot{\alpha}_2. \tag{2.25}$$

In this work, as mentioned earlier, the interfacial component and effects of stretching on the transition rate are not considered. Under these assumptions the melting rate for the second crystalline phase can be obtained by simplifying Eq. (1.85), and the resulting equation is:

$$\dot{\alpha}_2 = G_2(\alpha_2)^{k_2/m_2-1}\left(\frac{\theta - \theta_{r_2}}{\theta_{r_2}}\right)^{1/m_2-1} \tag{2.26}$$

Using Eq. (1.86) and substituting the values of the kinematical quantities given by Eqs. (2.5) and (2.6), the components of the Cauchy stress tensor reduce to:

$$\begin{aligned}
\sigma_{\vartheta\vartheta} &= -p + (1-\alpha_1(t)-\alpha_2(t))\mu_a\left(\tfrac{r}{R}\right)^2 + \mu_{c_1}\int_{t_{s_1}}^{t_{f_2}}\left(\tfrac{r(t)}{r(\tau)}\right)^2\tfrac{d\alpha_1}{d\tau}d\tau + \mu_{c_1 2}\int_{t_{s_1}}^{t_{f_2}}\left(\left(\tfrac{r(t)}{r(\tau)}\right)^4 - \left(\tfrac{r(t)}{r(\tau)}\right)^2\right)\tfrac{d\alpha_1}{d\tau}d\tau \\
&\quad + \mu_{c_2}\int_{t_{s_2}}^{\tau^{**}}\left(\tfrac{r(t)}{r(\tau)}\right)^2\tfrac{d\alpha_2}{d\tau}d\tau + \mu_{c_2 2}\int_{t_{s_2}}^{\tau^{**}}\left(\left(\tfrac{r(t)}{r(\tau)}\right)^4 - \left(\tfrac{r(t)}{r(\tau)}\right)^2\right)\tfrac{d\alpha_2}{d\tau}d\tau \\
\sigma_{rr} &= -p + (1-\alpha_1(t)-\alpha_2(t))\mu_a\left(\tfrac{R}{\Lambda r}\right)^2 + \mu_{c_1}\int_{t_{s_1}}^{t_{f_2}}\left(\tfrac{r(\tau)}{r(t)}\right)^2\tfrac{d\alpha_1}{d\tau}d\tau + \mu_{c_1 2}\int_{t_{s_1}}^{t_{f_2}}\left(\left(\tfrac{r(\tau)}{r(t)}\right)^4 - \left(\tfrac{r(\tau)}{r(t)}\right)^2\right)\tfrac{d\alpha_1}{d\tau}d\tau \\
&\quad + \mu_{c_2}\int_{t_{s_2}}^{\tau^{**}}\left(\tfrac{r(\tau)}{r(t)}\right)^2\tfrac{d\alpha_2}{d\tau}d\tau + \mu_{c_2 2}\int_{t_{s_2}}^{\tau^{**}}\left(\left(\tfrac{r(\tau)}{r(t)}\right)^4 - \left(\tfrac{r(\tau)}{r(t)}\right)^2\right)\tfrac{d\alpha_2}{d\tau}d\tau
\end{aligned} \tag{2.27}$$

with $\tau^{**} \in [t_{s_2}, t_{f_2}]$ *and* $\alpha_2(\tau^{**}) = \alpha_2(t)$. Using these values of stress the balance of linear momentum given by Eq. (2.11) can be simplified to give the pressure difference. It is important to note that the pressure difference here is exactly equal to zero.

3.2.8. Heating-2

During the second heating process, the material is heated above the first transition temperature θ_{r_1}, during this process crystalline phase-1 melts. This heating process is similar to the first heating process.

The energy equation reduces to:

$$\frac{\partial\theta}{\partial t} = \gamma\left(\frac{\partial^2\theta}{\partial r^2} + \frac{1}{r}\frac{\partial\theta}{\partial r}\right) - \frac{\Delta H_a}{C_a}\dot{\alpha}_1. \tag{2.28}$$

Using the same assumptions as the first heating process the crystallization rate for phase-1 can be obtained by simplifying Eq. (1.99), and the resulting equation is:

$$\dot{\alpha}_1 = G_1(\alpha_1)^{k_1/m_1-1}\left(\frac{\theta-\theta_{r_1}}{\theta_{r_1}}\right)^{1/m_1-1} \tag{2.29}$$

Using Eq. (1.100) and substituting the values of the kinematical quantities given by Eqs. (2.5) and (2.6), the components of the Cauchy stress tensor reduce to:

$$\begin{aligned}
\sigma_{\vartheta\vartheta} &= -p + (1-\alpha_1(t))\mu_a\left(\tfrac{r}{R}\right)^2 + \mu_{c_1}\int_{t_{s_1}}^{\tau^*}\left(\tfrac{r(t)}{r(\tau)}\right)^2\tfrac{d\alpha_1}{d\tau}d\tau + \mu_{c_12}\int_{t_{s_1}}^{\tau^*}\left(\left(\tfrac{r(t)}{r(\tau)}\right)^4 - \left(\tfrac{r(t)}{r(\tau)}\right)^2\right)\tfrac{d\alpha_1}{d\tau}d\tau \\
\sigma_{rr} &= -p + (1-\alpha_1(t))\mu_a\left(\tfrac{R}{\Lambda r}\right)^2 + \mu_{c_1}\int_{t_{s_1}}^{\tau^*}\left(\tfrac{r(\tau)}{r(t)}\right)^2\tfrac{d\alpha_1}{d\tau}d\tau + \mu_{c_12}\int_{t_{s_1}}^{\tau^*}\left(\left(\tfrac{r(\tau)}{r(t)}\right)^4 - \left(\tfrac{r(\tau)}{r(t)}\right)^2\right)\tfrac{d\alpha_1}{d\tau}d\tau
\end{aligned} \tag{2.30}$$

with, $\tau^* \in [t_{s_1}, t_{f_2}]$ *and* $\alpha_1(\tau^*) = \alpha_1(t)$. Using these values of stress and using the methodology used for heating-1 the pressure difference can be calculated. The pressure difference here is exactly zero as before. Using these equations, it is possible to solve the problem for the hollow cylindrical geometry and the prescribed motion. Since the aim here is to carry out a representative study to highlight the efficacy of the theory, all the equations are converted into a non-dimensional form.

3.3. Non-dimensional equations and solution methodology

In this section, key equations are prescribed in non-dimensional form for all the eight processes and the solution methodology used is discussed. The different physical variables encountered in this problem are non-dimensionalized (normalized) in the following manner:

$$\Delta P^* = \frac{\Delta P}{\mu_a}, \quad r^* = \frac{r}{R_1}, \quad R^* = \frac{R}{R_1}, \quad t^* = \frac{t}{(R^2{}_1/\gamma)} \tag{2.31}$$

$$\begin{aligned}
&Cooling-1 \quad \theta^* = \tfrac{\theta-\theta_{\min}}{\Delta\theta_{\max}}, \quad \Delta\theta_{\max} = \theta_{init} - \theta_{\min}, \\
&Cooling-2 \quad \theta^* = \tfrac{\theta-\theta_{\min}}{\Delta\theta_{\max}}, \quad \Delta\theta_{\max} = \theta_{init} - \theta_{\min}.
\end{aligned} \tag{2.32}$$

$$\begin{aligned}
&\mu^*{}_{c_1} = \tfrac{\mu_{c_1}}{\mu_a}, \quad \mu^*{}_{c_11} = \tfrac{\mu_{c_11}}{\mu_a} \quad and \quad \mu^*{}_{c_12} = \tfrac{\mu_{c_12}}{\mu_a}, \\
&\mu^*{}_{c_2} = \tfrac{\mu_{c_1}}{\mu_a}, \quad \mu^*{}_{c_12} = \tfrac{\mu_{c_21}}{\mu_a} \quad and \quad \mu^*{}_{c_12} = \tfrac{\mu_{c_22}}{\mu_a}.
\end{aligned} \tag{2.33}$$

For the sake of clarity we drop the * sign for the non-dimensional forms in the following derivation and calculation. In the above equation, θ_{init} is the initial temperature before both the cooling processes and is above the transition temperatures of phase-1 and phase-2. $\theta_{\min}$ is the lowest possible temperature and is below both the transition temperatures of phase-1 and phase-2.

During the loading-1 process the non-dimensional form of the key equation connecting the pressure difference and the radius at any given time can be written as:

$$\Delta P = \int_{r_1}^{r_2}\left(\frac{\left(\frac{r}{R}\right)^2 - \left(\frac{R}{\Lambda r}\right)^2}{r}\right) \tag{2.34}$$

The loading can be prescribed either by increasing the values of inner radius at every time step or by an internal pressure which is a function of time. If the loading process is prescribed by the internal pressure, then in the above equation, the left side is known. Now guessing the values for r_1, using Eq. (2.8) the right side can be integrated, this process continues till the correct value of r_1 is found. If the loading is defined by providing the inner radius as a function of time then using Eq. (2.8), numerical values of the radii for each node can be found. Once we know all the values using trapezoidal rule for integration, the pressure difference can be found easily. Using Eq. (2.33), the energy equation during cooling-1 can be written as:

$$\frac{\partial\theta}{\partial t} = \left(\frac{\partial^2\theta}{\partial r^2} + \frac{1}{r}\frac{\partial\theta}{\partial r}\right) + St\frac{d\alpha_1}{dt} \tag{2.35}$$

The boundary conditions are:

$$\frac{\partial\theta(r_1,t)}{\partial r}=0,\quad \frac{\partial\theta(r_2,t)}{\partial t}=-k, \tag{2.36}$$

where $St=\frac{\Delta H_a}{C_a\Delta\theta_{\max}}$ is the Stefan number and is associated with the phase change process and the initial temperature, θ_{init} is above both the transition temperatures. The equation governing the crystallization in its non-dimensional form can be written as:

$$\dot{\alpha}_1=\hat{G}_1(\alpha_{0_1}-\alpha_1)^{k_1/m_1-1}\left(\frac{\theta_{r_1}-\theta}{\theta_{r_1}+\theta_{\min}/\Delta\theta_{\max}}\right)^{1/m_1-1}\quad where\ \ \hat{G}_1=G_1\frac{R^2{}_1}{\gamma}. \tag{2.37}$$

The equation for the pressure difference during first cooling process after non-dimensionalizing reduces to

$$\Delta P=\int_{r_1}^{r_2}\times\left(\frac{(1-\alpha_1(t))\left(\left(\frac{r}{R}\right)^2-\left(\frac{1}{\Lambda}\frac{R}{r}\right)^2\right)+\mu_{c_1}\int_{t_{s_1}}^{t}\left(\left(\frac{r(t)}{r(\tau)}\right)^2-\left(\frac{r(\tau)}{r(t)}\right)^2\right)\frac{d\alpha_1}{d\tau}d\tau}{r}\right.$$
$$\left.\frac{+\int_{t_{s_1}}^{t}\left[\mu_{c_1 2}\left(\left(\frac{r(t)}{r(\tau)}\right)^4-\left(\frac{r(t)}{r(\tau)}\right)^2\right)-\mu_{c_1 1}\left(\left(\frac{r(\tau)}{r(t)}\right)^4-\left(\frac{r(\tau)}{r(t)}\right)^2\right)\frac{d\alpha_1}{d\tau}d\tau\right]}{r}dr\right) \tag{2.38}$$

We have divided the computational domain that ranges from inner radius R_1 to outer radius R_2 into several nodes. Using this grid and an explicit scheme for the diffusion equation we can find the temperature at every node. Once the temperature is known, the crystallinity of phase-1 can be found by solving the ordinary differential equation (Eq. (2.37)). While cooling there will be no change in the values of radii at different nodes if the shape of the material is held fixed. In such a scenario, Eq. (2.38) will be reduced to

$$\Delta P=\int_{r_1}^{r_2}\frac{\left[(1-\alpha_1(t))\left(\left(\frac{r}{R}\right)^2-\left(\frac{1}{\Lambda}\frac{R}{r}\right)^2\right)\right]}{r}dr \tag{2.39}$$

In order to find the pressure difference, the above equation is integrated using the trapezoidal rule.

The unloading-1 process is assumed to be isothermal and so there will be no change in the crystallinity i.e., no phase transition will occur. As the internal pressure reduces to match the external pressure the pressure difference gradually decreases. The equation connecting the radial location to the pressure difference, in dimensionless form is given by:

$$\Delta P=\int_{r_1}^{r_2}\times\left(\frac{(1-\alpha_1(t))\left(\left(\frac{r}{R}\right)^2-\left(\frac{1}{\Lambda}\frac{R}{r}\right)^2\right)+\mu_{c_1}\int_{t_{s_1}}^{t_{f_1}}\left(\left(\frac{r(t)}{r(\tau)}\right)^2-\left(\frac{r(\tau)}{r(t)}\right)^2\right)\frac{d\alpha_1}{d\tau}d\tau}{r}\right.$$
$$\left.\frac{+\int_{t_{s_1}}^{t_{f_1}}\left[\mu_{c_1 2}\left(\left(\frac{r(t)}{r(\tau)}\right)^4-\left(\frac{r(t)}{r(\tau)}\right)^2\right)-\mu_{c_1 1}\left(\left(\frac{r(\tau)}{r(t)}\right)^4-\left(\frac{r(\tau)}{r(t)}\right)^2\right)\frac{d\alpha_1}{d\tau}d\tau\right]}{r}dr\right) \tag{2.40}$$

Guessing the values for the inner radius of the hollow cylinder we can find the values of location at each nodal point using Eq. (2.8) . Using the Newton-Raphson scheme iterations are performed till the correct value of the radii are obtained that satisfy Eq. (2.40). During loading-2 the equation for pressure difference can be shown to be given by Eq. (2.40), this equation is solved using methodology similar to unloading-1. Using Eq. (2.33), the energy equation during the second cooling process (cooling-2) can be written as:

$$\frac{\partial\theta}{\partial t}=\left(\frac{\partial^2\theta}{\partial r^2}+\frac{1}{r}\frac{\partial\theta}{\partial r}\right)+St\frac{d\alpha_1}{dt}+St\frac{d\alpha_2}{dt} \tag{2.41}$$

The boundary conditions are:

$$\frac{\partial\theta(r_1,t)}{\partial r}=0,\quad \frac{\partial\theta(r_2,t)}{\partial t}=-k, \tag{2.42}$$

The equation governing the crystallization of crystalline phase-2 in its non-dimensional form can be written as:

$$\dot{\alpha}_2=\hat{G}_2(\alpha_{0_2}-\alpha_2)^{k_2/m_2-1}\left(\frac{\theta_{r_2}-\theta}{\theta_{r_2}+\theta_{\min}/\Delta\theta_{\max}}\right)^{1/m_2-1}\quad where\ \ \hat{G}_2=G_2\frac{R^2{}_1}{\gamma}. \tag{2.43}$$

The equation for the pressure difference during the second cooling process after non-dimensionalization reduces to:

$$\Delta P = \int_{r_1}^{r_2} \times \left(\begin{array}{l} \dfrac{(1-\alpha_1(t)-\alpha_2(t))\left(\left(\frac{r}{R}\right)^2-\left(\frac{1}{\Lambda}\frac{R}{r}\right)^2\right)+\mu_{c_1}\int_{t_{s_1}}^{t}\left(\left(\frac{r(t)}{r(\tau)}\right)^2-\left(\frac{r(\tau)}{r(t)}\right)^2\right)\frac{d\alpha_1}{d\tau}d\tau}{r} \\ \dfrac{+\int_{t_{s_1}}^{t}\left[\mu_{c_1 2}\left(\left(\frac{r(t)}{r(\tau)}\right)^4-\left(\frac{r(t)}{r(\tau)}\right)^2\right)-\mu_{c_1 1}\left(\left(\frac{r(\tau)}{r(t)}\right)^4-\left(\frac{r(\tau)}{r(t)}\right)^2\right)\frac{d\alpha_1}{d\tau}d\tau\right]}{r} \dfrac{+\mu_{c_2}\int_{t_{s_2}}^{t}\left(\left(\frac{r(t)}{r(\tau)}\right)^2-\left(\frac{r(\tau)}{r(t)}\right)^2\right)\frac{d\alpha_2}{d\tau}d\tau}{r} \\ \dfrac{+\int_{t_{s_2}}^{t}\left[\mu_{c_2 2}\left(\left(\frac{r(t)}{r(\tau)}\right)^4-\left(\frac{r(t)}{r(\tau)}\right)^2\right)-\mu_{c_2 1}\left(\left(\frac{r(\tau)}{r(t)}\right)^4-\left(\frac{r(\tau)}{r(t)}\right)^2\right)\frac{d\alpha_2}{d\tau}d\tau\right]}{r} dr \end{array} \right) \tag{2.44}$$

Crystallinity of phase-2 is solved for using methodology similar to cooling-1. During the second cooling process for the material, if the shape is kept fixed, there will be no change in the values of radii at different nodes. In such a scenario, Eq. (2.44) will be reduced to

$$\Delta P = \int_{r_1}^{r_2} \times \left(\begin{array}{l} \dfrac{(1-\alpha_1(t)-\alpha_2(t))\left(\left(\frac{r}{R}\right)^2-\left(\frac{1}{\Lambda}\frac{R}{r}\right)^2\right)+\mu_{c_1}\int_{t_{s_1}}^{t_{f_1}}\left(\left(\frac{r(t)}{r(\tau)}\right)^2-\left(\frac{r(\tau)}{r(t)}\right)^2\right)\frac{d\alpha_1}{d\tau}d\tau}{r} \\ \dfrac{+\int_{t_{s_1}}^{t_{f_1}}\left[\mu_{c_1 2}\left(\left(\frac{r(t)}{r(\tau)}\right)^4-\left(\frac{r(t)}{r(\tau)}\right)^2\right)-\mu_{c_1 1}\left(\left(\frac{r(\tau)}{r(t)}\right)^4-\left(\frac{r(\tau)}{r(t)}\right)^2\right)\frac{d\alpha_1}{d\tau}d\tau\right]}{r} \end{array} \right) \tag{2.45}$$

In order to find the pressure difference, the above equation is integrated using the trapezoidal rule. The equation for pressure difference during unloading-2 is similar to Eq. (2.44), the only difference being in the limits of integrals, the upper limit in this case is t_{f_2}. This equation is solved by adopting solution methodology similar to unloading-1.

The rate equation for phase-2 for the first heating process heating-1, along with the initial condition and boundary conditions, in its non-dimensional form, can be written as

$$\frac{\partial\theta}{\partial t} = \left(\frac{\partial^2\theta}{\partial r^2} + \frac{1}{r}\frac{\partial\theta}{\partial r}\right) - St\frac{d\alpha_2}{dt}. \tag{2.46}$$

The boundary conditions are:

$$\frac{\partial\theta(r_1,t)}{\partial r} = 0, \quad \frac{\partial\theta(r_2,t)}{\partial t} = k, \tag{2.47}$$

The temperature before heating everywhere is below the lower transition temperature. The temperature at every nodal point is obtained by solving the diffusion equation using an explicit scheme. Once the temperature is known, the non-dimensional equation for crystallization of phase-2, given below, can be solved for the crystallinity at each point.

$$\dot{\alpha}_2 = \hat{G}_2(\alpha_2)^{k_2/m_2-1}\left(\frac{\theta-\theta_{r_2}}{\theta_{r_2}+\theta_{\min}/\Delta\theta_{\max}}\right)^{1/m_2-1} \quad where \;\; \hat{G}_2 = G_2\frac{R^2{}_1}{\gamma}. \tag{2.48}$$

The balance of momentum equation in its non-dimensional form can be expressed as

$$\Delta P = \int_{r_1}^{r_2} \times \left(\begin{array}{l} \dfrac{(1-\alpha_1(t)-\alpha_2(t))\left(\left(\frac{r}{R}\right)^2-\left(\frac{1}{\Lambda}\frac{R}{r}\right)^2\right)+\mu_{c_1}\int_{t_{s_1}}^{t_{f_2}}\left(\left(\frac{r(t)}{r(\tau)}\right)^2-\left(\frac{r(\tau)}{r(t)}\right)^2\right)\frac{d\alpha_1}{d\tau}d\tau}{r} \\ \dfrac{+\int_{t_{s_1}}^{t_{f_2}}\left[\mu_{c_1 2}\left(\left(\frac{r(t)}{r(\tau)}\right)^4-\left(\frac{r(t)}{r(\tau)}\right)^2\right)-\mu_{c_1 1}\left(\left(\frac{r(\tau)}{r(t)}\right)^4-\left(\frac{r(\tau)}{r(t)}\right)^2\right)\frac{d\alpha_1}{d\tau}d\tau\right]}{r} \dfrac{+\mu_{c_2}\int_{t_{s_2}}^{t^{**}}\left(\left(\frac{r(t)}{r(\tau)}\right)^2-\left(\frac{r(\tau)}{r(t)}\right)^2\right)\frac{d\alpha_2}{d\tau}d\tau}{r} \\ \dfrac{+\int_{t_{s_2}}^{t^{**}}\left[\mu_{c_2 2}\left(\left(\frac{r(t)}{r(\tau)}\right)^4-\left(\frac{r(t)}{r(\tau)}\right)^2\right)-\mu_{c_2 1}\left(\left(\frac{r(\tau)}{r(t)}\right)^4-\left(\frac{r(\tau)}{r(t)}\right)^2\right)\frac{d\alpha_2}{d\tau}d\tau\right]}{r} dr \end{array} \right) \tag{2.49}$$

Using the same solution process as was used for finding the location of a particle during the unloading processes, Eq. (2.49) can be solved. For the second heating process heating-2, the rate equation for phase-1 along with the initial condition and boundary conditions, in its non-dimensional form, can be written as

$$\frac{\partial\theta}{\partial t} = \left(\frac{\partial^2\theta}{\partial r^2} + \frac{1}{r}\frac{\partial\theta}{\partial r}\right) - St\frac{d\alpha_1}{dt} \tag{2.50}$$

The boundary conditions are:

$$\frac{\partial\theta(r_1,t)}{\partial r} = 0, \quad \frac{\partial\theta(r_2,t)}{\partial t} = k, \tag{2.51}$$

Table 1
Material constants and parameters used for the simulation.

Parameter	Value	Unit	Description
R_1	1	cm	Inner radius of the cylinder
R_2	2	cm	Outer radius of the cylinder
H	1	cm	Length of the cylinder
Λ	1.1	Dimensionless	Elongation of the cylinder
θ_{r_1}	90	Celsius	Transition temperature of crystalline phase-1
θ_{r_2}	60	Celsius	Transition temperature of crystalline phase-2
θ_{init}	100	Celsius	Initial temperature
$\Delta\theta_{\max}$	100	Kelvin	Maximum temperature change
ΔH_a	27	J/g	Latent heat
C_a	3.1	J/g	Specific heat
ρ	1.13	g/cc	Density of the material
$\hat{G}_1$	100	Dimensionless	Parameters for the
m_1	0.75	Dimensionless	crystallization rate of
k_1	0.2	Dimensionless	crystalline phase-1
$\hat{G}_2$	280	Dimensionless	Parameters for the
m_2	0.75	Dimensionless	crystallization rate of
k_2	0.2	Dimensionless	crystalline phase-2
$\mu^*_{c_1}$	100	Dimensionless	Normalized shear moduli of
$\mu^*_{c_1 1}$	2	Dimensionless	crystalline phase-1
$\mu^*_{c_1 1}$	2	Dimensionless	
$\mu^*_{c_2}$	100	Dimensionless	Normalized shear moduli of
$\mu^*_{c_2 1}$	2	Dimensionless	crystalline phase-2
$\mu^*_{c_2 2}$	2	Dimensionless	

The temperature before the second heating process at all points is below the transition temperature of the first phase. The temperature at every nodal point is obtained by using the same technique as heating −1. Once the temperature is known, the non-dimensional equation for crystallization of phase-1, given below, can be solved for crystallinity at each point.

$$\dot{\alpha}_1 = \hat{G}_1(\alpha_1)^{k_1/m_1-1}\left(\frac{\theta-\theta_{r_1}}{\theta_{r_1}+\theta_{\min}/\Delta\theta_{\max}}\right)^{1/m_1-1} \quad \text{where } \hat{G}_1 = G_1\frac{R^2 1}{\gamma}. \tag{2.52}$$

The balance of momentum equation in its non-dimensional form can be expressed as

$$\Delta P = \int_{r_1}^{r_2}\times\left(\frac{(1-\alpha_1(t))\left(\left(\frac{r}{R}\right)^2-\left(\frac{1}{\Lambda}\frac{R}{r}\right)^2\right)+\mu_{c_1}\int_{t_{s_1}}^{t^*}\left(\left(\frac{r(t)}{r(\tau)}\right)^2-\left(\frac{r(\tau)}{r(t)}\right)^2\right)\frac{d\alpha_1}{d\tau}d\tau}{r}\right.$$
$$\left.+\frac{\int_{t_{s_1}}^{t^*}\left[\mu_{c_1 2}\left(\left(\frac{r(t)}{r(\tau)}\right)^4-\left(\frac{r(t)}{r(\tau)}\right)^2\right)-\mu_{c_1 1}\left(\left(\frac{r(\tau)}{r(t)}\right)^4-\left(\frac{r(\tau)}{r(t)}\right)^2\right)\frac{d\alpha_1}{d\tau}d\tau\right]}{r}dr \tag{2.53}$$

Using the same solution practice that was used for finding the location of the particle during the unloading-1 process, Eq. (2.53) can be solved.

3.4. Results

In this section, the main results obtained by solving the theory have been discussed. Two classes of boundary value problems have been studied here for triple shape memory polymers; crystallization under constant strain and crystallization under constant stress. Parameters used for the simulation are shown in Table 1 unless they are given separately.

The first sets of results discussed are for the case of inflation-extension of a hollow cylinder, undergoing crystallization under constant strain. During the triple shape memory cycle the graph of the variation of the temperature with time for different locations is shown in Fig. 6. The cylinder is cooled or heated by varying the temperature at the outer radius while the inner radius is kept insulated. During cooling-1, once the temperature drops below the first transition temperature θ_{r_1}, crystallization of phase-1 begins. During cooling-2, when the temperature drops below the second transition temperature θ_{r_2}, phase-2 starts crystallizing and phase-1 continues to crystallize at the lower temperature. The variation of the crystallinity with time for a triple shape memory cycle is depicted in Fig. 7. The pressure versus radius at a material point, at a particular radial location in the cylinder for a triple shape memory cycle of deformation is shown in Fig. 8. Initially with the increase in pressure, the radius increases as the polymer deforms. The stiffness of the material increases once the first crystallization is initiated, and for maintaining the same radius, a lower pressure is needed. On unloading after the first crystallization process a small retraction is observed, i.e. the material remains in its first temporary shape. During the second loading process, the material is stiffer due to the presence of the crystalline phase-1 and a higher pressure is required for an increase in the radius as the polymer deforms, as compared to the first loading. During the second crystallization

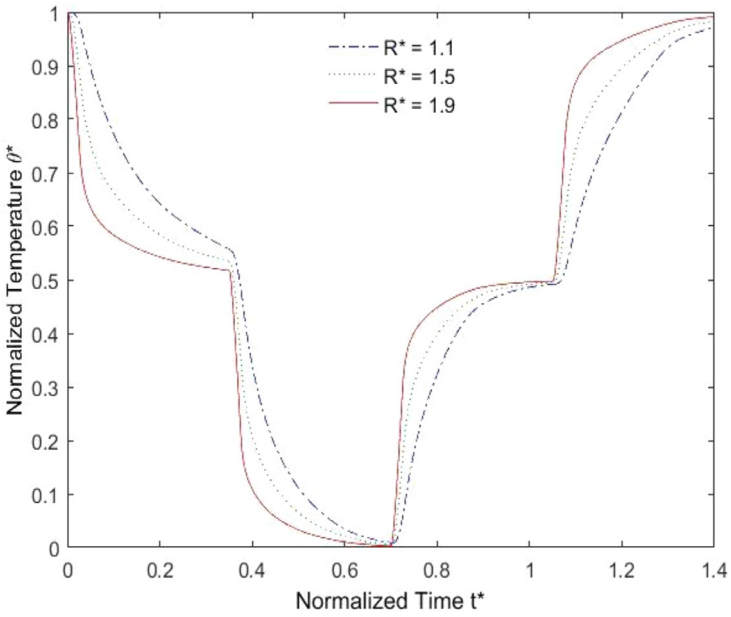

Fig. 6. Temperature variation with time (shape is kept constant while cooling). Parameters used for the simulation are given in Table 1.

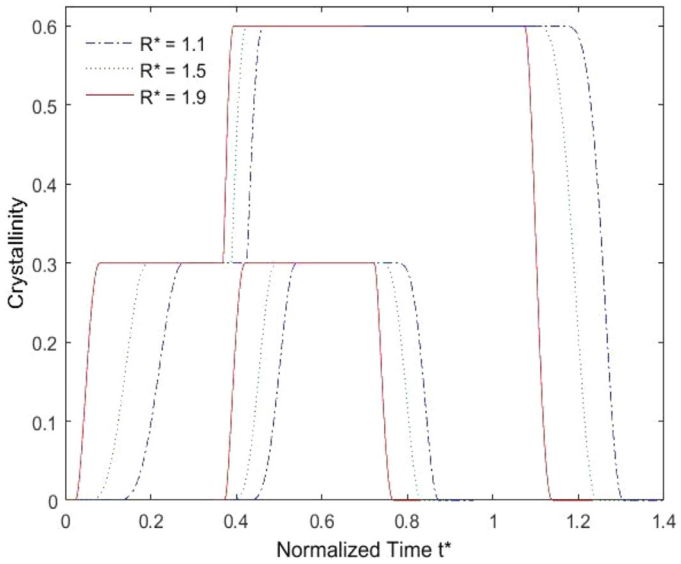

Fig. 7. Crystallinity variation with time (shape is kept constant while cooling). Parameters used for the simulation are given in Table 1.

process the drop in the pressure is lower as compared to the first crystallization process as the material is stiffer due to the presence of the crystalline phase. On unloading after the second crystallization process, again a small retraction is observed, i.e. the material remains in its second temporary shape. On subsequent heating the material goes back to its original shape. This triple shape cycle can be seen in Fig. 8.

The second set of results is for a case where the pressure difference is kept constant while cooling (i.e. during crystallization). Figs. 9 and 10 show the variation of the temperature and crystallinity with time, for a triple shape cycle. As temperature decreases below the first recovery temperature, crystallinity of phase-1 increases and the semi-crystalline mixture forms. As temperature decreases below the second recovery temperature, crystallinity of both the phases increases simultaneously. When crystals form they are stress free, however as the crystallization is taking place at constant pressure, these crystals deform. Hence, in Fig. 11, during both the crystallization processes, once crystallization is initiated a steady increase in the radius can be seen. After both the unloading processes the sample retracts by a small but finite amount because of the increase in the stiffness and the temporary shapes are preserved. Upon heating, the crystals undergo transition

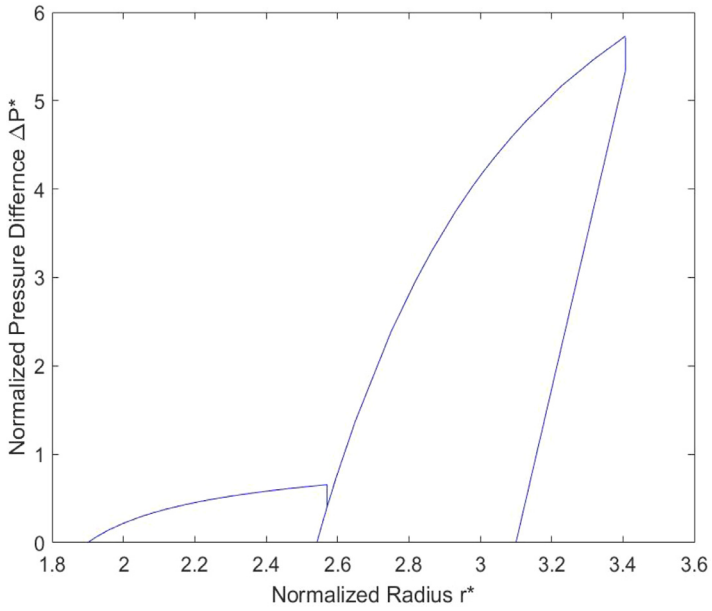

Fig. 8. Pressure difference versus Radii at $R_1 = 1.9$ (Shape is kept constant while cooling). Parameters used for the simulation are given in Table 1.

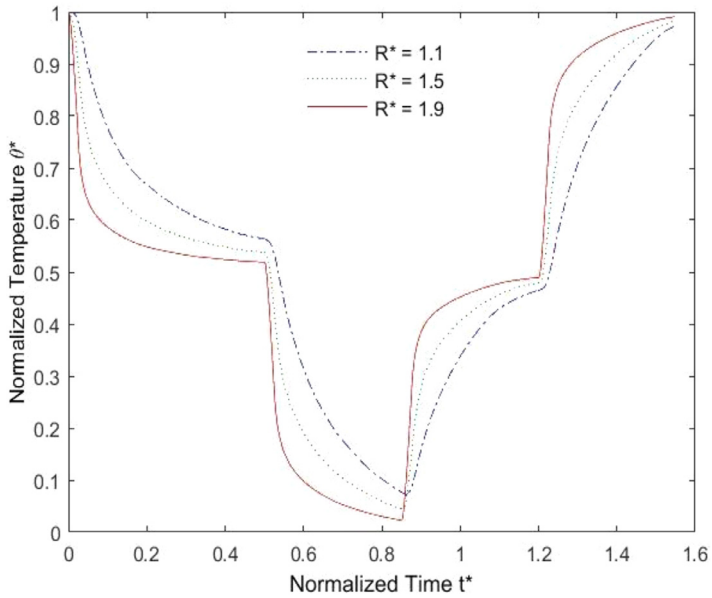

Fig. 9. Temperature variation with time (pressure difference is kept constant while cooling). Parameters used for the simulation are given in Table 1.

to the amorphous phase and the material returns towards the first temporary shape due to the first crystalline phase and subsequently to the original shape due to the cross-links that are present in the network in the amorphous region.

The third case of results discussed is for uni-axial extension; for details of the modeling of the mechanics associated with a uni-axial deformation cycle see [1]. We have compared the results of the simulation of the aforementioned case with experimental data presented in Zotzmann et al. (2010). Note that for the data presented the material does not exhibit viscoelastic behavior or creep. The material constants used are consistent with the data presented. The plot of stretch versus temperature is shown in Fig. 12, as can be seen the predictions compare very well with experimental data. Here, the material is cooled from a temperature above the second recovery temperature θ_{r_2}, to a temperature below the first recovery temperature θ_{r_1} in one step. During the cooling process both the phases crystallize; as the load is held constant during crystallization, the material undergoes extension. On heating above the first recovery temperature, the first phase melts. As the load is held constant during the process, melting of the crystalline phase leads to contraction of the material. On further heating above the second recovery temperature, the first phase melts and the material returns to the original shape.

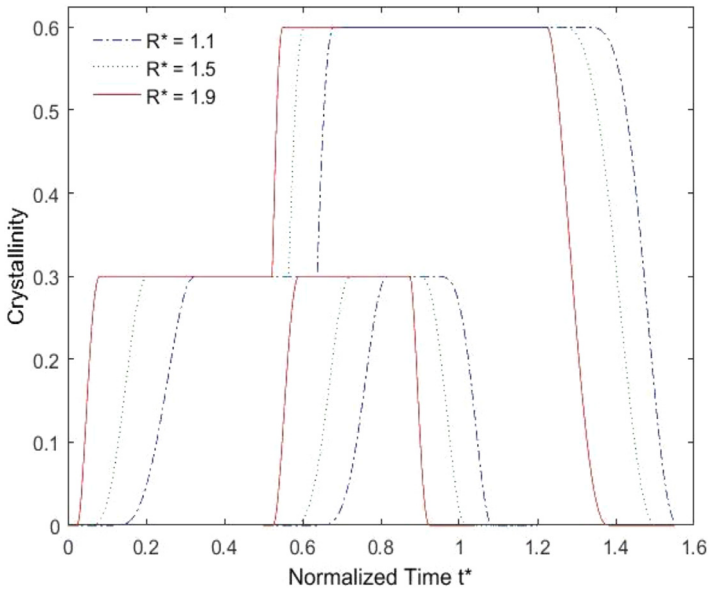

Fig. 10. Crystallinity variation with time (pressure difference is kept constant while cooling). Parameters used for the simulation are given in Table 1.

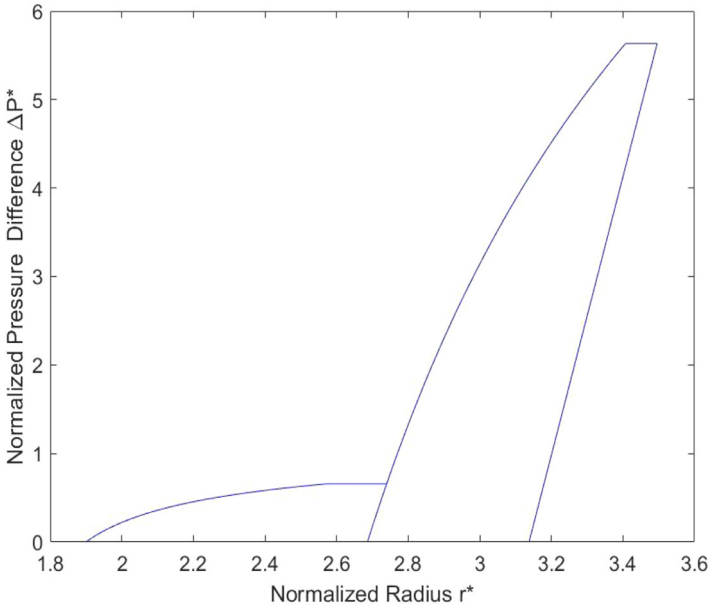

Fig. 11. Pressure difference versus Radii at $R_1 = 1.9$(pressure difference is kept constant while cooling). Parameters used for the simulation are given in Table 1.

The material exhibits two stable temporary shapes or a triple shape behavior during the heating process. The load is held constant during the entire deformation cycle. The fourth case of results discussed is for uni-axial extension, the stretch is plotted versus temperature change of the material during the shape recovery process. We have compared the results of the simulation of this case with the experimental data presented in Zotzmann et al. (2011), for the data presented the material does not exhibit viscoelastic behavior or creep. The material constants used are consistent with the data presented. The plot of stretch versus temperature is shown in Fig. 13, as can be seen the predictions compare well with the experimental data. The initial state is the second temporary shape, where the temperature is below the second recovery temperature θ_{r_2}. On heating aboveθ_{r_2}, the second crystalline phase formed at the lower temperature begins to melt, and the material starts to revert towards the first temporary shape. On further heating above the first recovery temperature θ_{r_1}, the first crystalline phase formed at the lower temperature and at the higher temperature melts. This leads to recovery of the permanent shape.

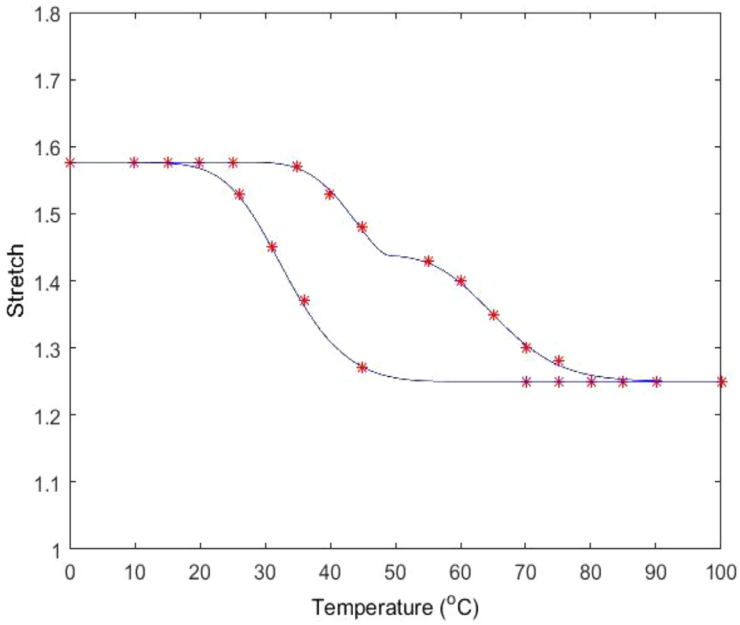

Fig. 12. Temperature (°C) variation with stretch, * indicates experimental data from (Zotzmann et al.). Parameters used for the simulation are, $G_1 = 300$, $G_2 = 300$, $m_1 = 1.3$, $k_1 = 0.3$, $m_2 = 1.3$, $k_2 = 0.3$, $\alpha_{01} = 0.45$, $\alpha_{02} = 0.15$, and the remaining parameters are given in Table 1.

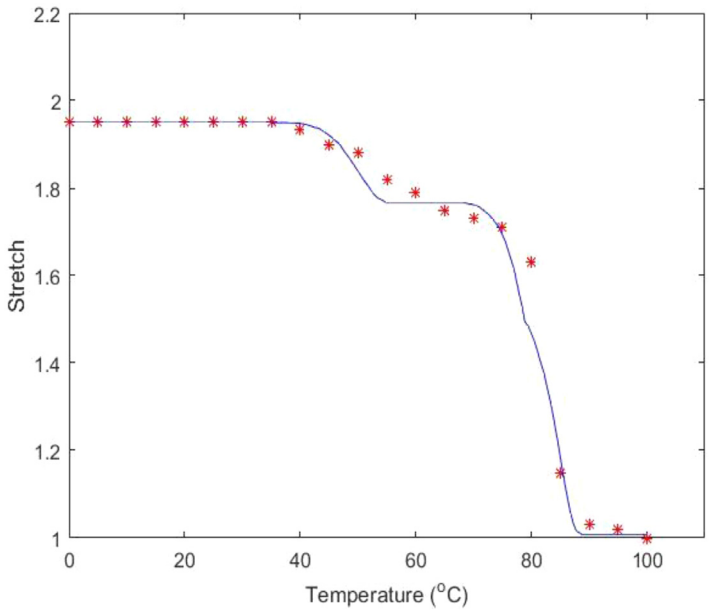

Fig. 13. Temperature (°C) variation with stretch during melting, * indicates experimental data from (Zotzmann et al.). Parameters used for the simulation are, $G_1 = 150$, $G_2 = 150$, $m_1 = 1.3$, $k_1 = 0.25$, $m_2 = 1.3$, $k_2 = 0.25$, $\alpha_{01} = 0.4$, $\alpha_{02} = 0.25$, and the remaining parameters are given in Table 1.

4. Conclusion

In this work we have developed constitutive equations to model triple shape memory polymers in a full thermodynamic setting. The model has been developed using the theory of multiple natural configurations. The model has been applied to solve for typical analytically tractable boundary value problems. The theory seems to predict results that are consistent with physical expectations. The proposed theory is built upon solid foundations as it fits in with a general framework developed to describe materials that are subject to disparate entropy producing processes. It is expected that his work will aid in further understanding the behavior of these novel materials undergoing complex deformations. Additionally, these

models can be used to simulate possible applications using these materials, aiding in the design and development of devices utilizing TSMPs.

References

Anand, L., et al. (2010). A large-deformation theory for thermally-actuated shape-memory polymers and its application. *ASME 2010 international mechanical engineering congress and exposition*. American Society of Mechanical Engineers.

Atkin, R. J., & Craine, R. E. (1976). Continuum theory of mixtures: Basic theory and historical development. *Quarterly Journal of Mechanics and Applied Mathematics, 29*(2), 153–207.

Baer, G., Wilson, T. S., Matthews, D. L., & Maitland, D. J. (2007a). Shape-memory behavior of thermally stimulated polyurethane for medical applications. *Journal of Applied Polymer Science, 103*(6), 3882–3892.

Bare, G. M., Small, W., Wilson, T. S., Benett, W. J., Matthews, D. L., & Hartman, J. M. (2007b). Fabrication and in vitro deployment of a laser-activated shape memory polymer vascular stent. *BioMedical Engineering Online, 6*, 6–43.

Barot, G., & Rao, I. J. (2006). Constitutive modeling of the mechanics associated with crystallizable shape memory polymers. *Zeitschrift fur Angewandte Mathematik und Physik, 57*(4), 652–681.

Barot, G., Rao, I. J., & Rajagopal, K. R. (2008). A thermodynamic framework for the modeling of crystallizable shape memory polymers. *International Journal of Engineering Science, 46*(4), 325–351.

Behl, M., & Lendlein, A. (2012). Triple-shape polymers. *Journal of Material Chemistry, 20*, 3332–3334.

Behl, M., et al. (2009a). Dual and triple shape capability of AB polymer networks based on poly(ε-caprolactone)dimethacrylates. In *Proceedings of the materials research society symposium*.

Behl, M., et al. (2009b). One-step process for creating triple-shape capability of AB polymer networks. *Advanced Functional Materials, 19*(1), 102–108.

Bellin, I., et al. (2006). Polymeric triple-shape materials.*: 103(48)* (pp. 18043–18047).

Boatti, E., Scalet, G., & Auricchio, F. (2016). A three-dimensional finite-strain phenomenological model for shape-memory polymers: Formulation, numerical simulations, and comparison with experimental data. *International Journal of Plasticity, 83*, 153–177.

Bowen, R. M. (1976). Theory of mixtures. *Continuum Physics, 3*, 1–127.

Cui, F., Moon, S., & Rao, I. J. (2016). Modeling the viscoelastic behavior of amorphous shape memory polymers at an elevated temperature. *Fluids, 1*(2), 15.

Cui, F., Moon, S., & Joga Rao, I. (2017). Modeling the mechanical behavior of crystallizable shape memory polymers: Incorporating temperature-dependent viscoelasticity. *International Journal of Advances in Engineering Sciences and Applied Mathematics, 9*(1), 21–29.

Ge, Q., Yu, K., Ding, Y., & Qi, H. J. (2012). Prediction of temperature-dependent free recovery behaviors of amorphous shape memory polymers. *Soft Matter, 8*(43), 11098–11105.

Gedde, U. W. (1999). *Polymer Physics*. Netherlands: Springer.

Green, A. E., & Naghdi, P. M. (1977). On thermodynamics and the nature of the second law. *Proceedings of the Royal Society of London Series A, 357*(1690), 253–270.

Hamel, C. M., Cui, F., & Chester, S. A. (2017). A finite element method for light activated shape-memory polymers. *International Journal for Numerical Methods in Engineering, 111*(5), 447–473.

Heuchel, M., Sauter, T., Kartz, K., & Lendlein, A. (2013). Thermally induced shape-memory effects in polymers: Quantification and related modeling approaches. *Journal of Polymer Science, Part B: Polymer Physics, 51*(8), 621–637.

Hu, J., Meng, H., Li, G., & Ibekwe, S. I. (2012a). A review of stimuli-responsive polymers for smart textile applications. *Smart Materials and Structures, 21*(5), 053001.

Hu, J., Zhu, Y., Huang, H., & Lu, J. (2012b). Recent advances in shape-memory polymers: Structure, mechanism, functionality, modeling and applications. *Progress in Polymer Science, 37*(12), 1720–1763.

Irie, M. (1998). Shape memory polymers. *Shape Memory Materials, 28*, 203–219.

Kannan, K., & Rajagopal, K. R. (2005). Simulation of fiber spinning including flow-induced crystallization. *Journal of Rheology, 49*(3), 683–703.

Kannan, K., Rao, I. J., & Rajagopal, K. R. (2002). A thermomechanical framework for the glass transition phenomenon in certain polymers and its application to fiber spinning. *Journal of Rheology, 46*(4), 977–999.

Kannan, K., Rao, I. J., & Rajagopal, K. R. (2006). A thermodynamic framework for describing solidification of polymer melts. *Journal of Engineering Materials and Technology, Transactions of the ASME, 128*(1), 55–63.

Kim, B. K., Lee, S. Y., & Xu, M. (1996). Polyurethanes having shape memory effects. *Polymer, 37*(26), 5781–5793.

Kim, B. K., Lee, S. Y., Lee, S. J., Baek, S. H., Choi, Y. J., Lee, J. O., et al. (1998). Polyurethane ionomers having shape memory effects. *Polymer, 39*(13), 2803–2808.

Kim, B. K., Lee, S. Y., & Xu, M. (2000). Shape-memory behavior of segmented polyurethanes with an amorphous reversible phase: The effect of block length and content. *Journal of Polymer Science, Part B: Polymer Physics, 38*(20), 2652–2657.

Lendlein, A., & Kelch, S. (2002). Shape-memory polymers. *Angewandte Chemie - International Edition, 41*(12), 2035–2057.

Lendlein, A., & Langer, R. (2002). Biodegradable, elastic shape-memory polymers for potential biomedical applications. *Science, 296*(5573), 1673–1676.

Lendlein, A., & Sauter, T. (2013). Shape-memory effect in polymers. *Macromolecular Chemistry and Physics, 214*(11), 1175–1177.

Lendlein, A., Schmidt, A. M., & Langer, R. (2001). AB-polymer networks based on oligo(ε-caprolactone) segments showing shape-menory properties.*: 98(3)* (pp. 842–847).

Lendlein, A., Behl, M., Hiebl, B., & Wischke, C. (2010). Shape-memory polymers as a technology platform for biomedical applications. *Expert Review of Medical Devices, 7*(3), 357–379.

Leng, J., Lan, X., Liu, Y., & Du, S. (2011). Shape-memory polymers and their composites: Stimulus methods and applications. *Progress in Materials Science, 56*(7), 1077–1135.

Li, F., Zhang, X., Hou, J., Xu, M., Luo, X., Ma, D., & Kim, B. K. (1997). Studies on thermally stimulated shape memory effect of segmented polyurethanes. *Journal of Applied Polymer Science, 64*(8), 1511–1516.

Li, Y., He, Y., & Liu, Z. (2017). A viscoelastic constitutive model for shape memory polymers based on multiplicative decompositions of the deformation gradient. *International Journal of Plasticity, 91*, 300–317.

Lin, J. R., & Chen, L. W. (1999). Shape-memorized crosslinked ester-type polyurethane and its mechanical viscoelastic model. *Journal of Applied Polymer Science, 73*(7), 1305–1319.

Long, K. N., Dunn, M. L., & Jerry Qi, H. (2010). Mechanics of soft active materials with phase evolution. *International Journal of Plasticity, 26*(4), 603–616.

Long, R., Qi, H. J., & Dunn, M. L. (2013). Thermodynamics and mechanics of photochemcially reacting polymers. *Journal of the Mechanics and Physics of Solids, 61*(11), 2212–2239.

Mather, P. T., Luo, X., & Rousseau, I. A. (2009). Shape memory polymer research. *Annual Review of Materials Research*, 445–471.

Mitchell, G. R., Davis, F. J., & Guo, W. (1993). Strain-induced transitions in liquid-crystal elastomers. *Physical Review Letters, 71*(18), 2947–2950.

Monkman, G. J. (2000). Advances in shape memory polymer actuation. *Mechatronics, 10*(4), 489–498.

Moon, S., Cui, F., & Rao, I. J. (2015). Constitutive modeling of the mechanics associated with triple shape memory polymers. *International Journal of Engineering Science, 96*, 86–110.

Moon, S., Rao, J., & Chester, S. (2016). Triple shape memory polymers: Constitutive modeling and numerical simulation. *Journal of Applied Mechanics, 83*(7), 071008.

Poilane, C., Delobelle, P., Lexcellent, C., Hayashi, S., & Tobushi, H. (2000). Analysis of the mechanical behavior of shape memory polymer membranes by nanoindentation, bulging and point membrane deflection tests. *Thin Solid Films, 379*(1-2), 156–165.

Rajagopal, K. R., & Srinivasa, A. R. (1995). On the inelastic behavior of solids - Part 1: Twinning. *International Journal of Plasticity, 11*(6), 653–678.

Rajagopal, K. R., & Srinivasa, A. R. (1998). Mechanics of the inelastic behavior of materials - Part 1, theoretical underpinnings. *International Journal of Plasticity, 14*(10-11), 945–967.
Rajagopal, K. R., & Srinivasa, A. R. (1999). On the thermomechanics of shape memory wires. *Zeitschrift fur Angewandte Mathematik und Physik, 50*(3), 459–496.
Rajagopal, K. R., & Srinivasa, A. R. (2000). A thermodynamic frame work for rate type fluid models. *Journal of Non-Newtonian Fluid Mechanics, 88*(3), 207–227.
Rajagopal, K. R., & Tao, L. (1995). Mechanics of Mixtures, World Scientific Publishing: Singapore-New Jersey-London-Hong Kong.
Rajagopal, K. R., & Wineman, A. S. (1992). A constitutive equation for nonlinear solids which undergo deformation induced microstructural changes. *International Journal of Plasticity, 8*(4), 385–395.
Rajagopal, K. R. (1995). Multiple configurations in continuum mechanics. *Multiple Configurations in Continuum Mechanics*.
Rao, I. J., & Rajagopal, K. R. (2000). Phenomenological modeling of polymer crystallization using the notion of multiple natural configurations. *Interfaces and Free Boundaries, 2*(1), 73–94.
Rao, I. J., & Rajagopal, K. R. (2002). A thermodynamic framework for the study of crystallization in polymers. *Zeitschrift fur Angewandte Mathematik und Physik, 53*(3), 365–406.
Rao, I. J., & Rajagopal, K. R. (2004). On the modeling of quiescent crystallization of polymer melts. *Polymer Engineering and Science, 44*(1), 123–130.
Rao, I. J., & Rajagopal, K. R. (2005). Simulation of the film blowing process for semicrystalline polymers. *Mechanics of Advanced Materials and Structures, 12*(2), 129–146.
Rao, I. J., & Rajagopal, K. R. (2007). The status of the K-BKZ model within the framework of materials with multiple natural configurations. *Journal of Non-Newtonian Fluid Mechanics, 141*(2-3), 79–84.
Reyntjens, W. G., Du Prez, F. E., & Goethals, E. J. (1999). Polymer networks containing crystallizable poly(octadecyl vinyl ether) segments for shape-memory materials. *Macromolecular Rapid Communications, 20*(5), 251–255.
Serrano, M. C., & Ameer, G. A. (2012). Recent insights into the biomedical applications of shape-memory polymers. *Macromolecular Bioscience, 12*(9), 1156–1171.
Sisson, A. L., & Lendlein, A. (2012). Advances in actively moving polymers. *Macromolecular Materials and Engineering, 297*(12), 1135–1137.
Sodhi, J. S., & Rao, I. J. (2010). Modeling the mechanics of light activated shape memory polymers. *International Journal of Engineering Science, 48*(11), 1576–1589.
Spencer, A. J. M. (1972). *Deformation of fibre-reinforced material,* (p. 128). Oxford: Oxford Univ. Press. New York.
Srivastava, V., Chester, S. A., & Anand, L. (2010). Thermally actuated shape-memory polymers: Experiments, theory, and numerical simulations. *Journal of the Mechanics and Physics of Solids, 58*(8), 1100–1124.
Sun, L., Huang, W. M., Ding, Z., Zhao, Y., Wang, C. C., Purnawali, H., et al. (2012). Stimulus-responsive shape memory materials: A review. *Materials and Design, 33*(1), 577–640.
Tey, S. J., Huang, W. M., & Sokolowski, W. M. (2001). Influence of long-term storage in cold hibernation on strain recovery and recovery stress of polyurethane shape memory polymer foam. *Smart Materials and Structures, 10*(2), 321–325.
Tobushi, H., Hara, H., Yamada, E., & Hayashi, S. (1996). Thermomechanical properties in a thin film of shape memory polymer of polyurethane series. *Smart Materials and Structures, 5*(4), 483–491.
Truesdell, C. (1957). Sulle basi della thermomeccanica. *Rendiconti Lincei, 22*(8), 33–38.
Wache, H. M., et al. (2003). Development of a polymer stent with shape memory effect as a drug delivery system. *Journal of Materials Science: Materials in Medicine, 14*(2), 109–112.
Wang, M., & Zhang, L. (1999). Recovery as a Measure of Oriented Crystalline Structure in Poly(ether ester)s Based on Poly(ethylene oxide) and Poly(ethylene terephthalate) Used as Shape Memory Polymers. *Journal of Polymer Science, Part B: Polymer Physics, 37*(2), 101–112.
Wang, X. M., Xu, B. X., & Yue, Z. F. (2008). Micromechanical modelling of the effect of plastic deformation on the mechanical behaviour in pseudoelastic shape memory alloys. *International Journal of Plasticity, 24*(8), 1307–1332.
Ward, S., Singhal, P., Wilson, T. S., & Maitland, D. J. (2010). Biomedical applications of thermally activated shape memory polymers. *Journal of Materials Chemistry, 20*(17), 3356–3366.
Westbrook, K. K., Parakh, V., Chung, T., Mather, P. T., Wan, L. C., Dunn, M. L., et al. (2010). Constitutive modeling of shape memory effects in semicrystalline polymers with stretch induced crystallization. *Journal of Engineering Materials and Technology, 132*(4), 041010.
Xiao, R., & Nguyen, T. D. (2015). An effective temperature theory for the nonequilibrium behavior of amorphous polymers. *Journal of the Mechanics and Physics of Solids, 82*, 62–81.
Xiao, R., Guo, J., & Nguyen, T. D. (2015). Modeling the multiple shape memory effect and temperature memory effect in amorphous polymers. *RSC Advances, 5*(1), 416–423.
Xie, T. (2011). Recent advances in polymer shape memory. *Polymer, 52*(22), 4985–5000.
Yakacki, C. M., Nguyen, T. D., Likos, R., & Gall, K. (2011). Impact of shape-memory programming on mechanically-driven recovery in polymers. *Polymer, 52*(21), 4947–4954.
Yu, K., Xie, T., Jinsong, L., & Qi, H. J. (2012). Mechanisms of multi-shape memory effects and associated energy release in shape memory polymers. *Soft Matter, 8*(20), 5687–5695.
Yuan, Z., Muliana, A., & Rajagopal, K. R. (2017). Modeling the response of light-activated shape memory polymers. *Mathematics and Mechanics of Solids, 22*(5), 1116–1143.
Zhao, Q., Behl, M., & Lendlein, A. (2013). Shape-memory polymers with multiple transitions: Complex actively moving polymers. *Soft Matter, 9*(6), 1744–1755.
Zhi, y., Muliana, A., & Rajagopal, K. (2017). Quasi-linear viscoelastic modeling of light-activated shape memory polymers. *Journal of Intelligent Material Systems and Structures, 28*(18) P. 1045389X17689936.
Zotzmann, J., Behl, M., Feng, Y., & Lendlein, A. (2010a). Copolymer networks based on poly(ω-pentadecalactone) and poly(ε-caprolactone)segments as a versatile triple-shape polymer system. *Advanced Functional Materials, 20*(20), 3583–3594.
Zotzmann, J., Behl, M., Hofmann, D., & Lendlein, A. (2010b). Reversible triple-shape effect of polymer networks containing polypentadecalactone- and poly(ε-caprolactone)-segments. *Advanced Materials, 22*(31), 3424–3429.
Zotzmann, J., Behl, M., & Lendlein, A. (2011). The influence of programming conditions on the triple-shape effect of copolymer networks with poly(ω-pentadecalactone) and poly(ε- caprolactone) as switching segments. *Macromolecular Symposia, 309-310*(1), 147–153.